

Review

Unmanned Aerial Vehicles (UAVs) in Landslide Investigation and Monitoring: A Review

Jianwei Sun, Guoqin Yuan, Laiyun Song and Hongwen Zhang *

Key Laboratory of Airborne Optical Imaging and Measurement, Changchun Institute of Optics, Fine Mechanics and Physics, Chinese Academy of Sciences, Changchun 130033, China; sunjianwei@ciomp.ac.cn (J.S.); yuanguoqin@ciomp.ac.cn (G.Y.); songlaiyun@ciomp.ac.cn (L.S.)

* Correspondence: zhanghongwen@ciomp.ac.cn

Abstract: Over the past decade, Unmanned Aerial Vehicles (UAVs) have emerged as essential tools for landslide studies, particularly in on-site investigations. This paper reviews UAV applications in landslide studies, with a focus on static geological characteristics, monitoring temporal and spatial dynamics, and responses post-events. We discuss the functions and limitations of various types of UAVs and sensors (RGB cameras, multi-spectral cameras, thermal IR cameras, SAR, LiDAR), outlining their roles and data processing methods in landslide applications. This review focuses on the UAVs' roles in landslide geology surveys, emphasizing landslide mapping, modeling and characterization. For change monitoring, it provides an overview of the temporal and spatial evolution through UAV-based monitoring, shedding light on dynamic landslide processes. Moreover, this paper underscores UAVs' crucial role in emergent response scenarios, detailing strategies and automated detection using machine learning algorithms. The discussion on challenges and opportunities highlights the need for ongoing UAV technology advancements, addressing regulatory hurdles, hover time limitations, 3D reconstruction accuracy and potential integration with technologies like UAV swarms.

Keywords: UAVs; landslide; remote sensing; photogrammetry



Citation: Sun, J.; Song, L.; Yuan, G.; Zhang, H. Unmanned Aerial Vehicles (UAVs) in Landslide Investigation and Monitoring: A Review. *Drones* **2024**, *8*, 30. <https://doi.org/10.3390/drones8010030>

Academic Editors: Vasil Yordanov, Luigi Barazzetti, Maria Antonia Brovelli

Received: 22 December 2023

Revised: 16 January 2024

Accepted: 17 January 2024

Published: 22 January 2024



Copyright: © 2024 by the authors. Licensee MDPI, Basel, Switzerland. This article is an open access article distributed under the terms and conditions of the Creative Commons Attribution (CC BY) license (<https://creativecommons.org/licenses/by/4.0/>).

1. Introduction

Unmanned aerial vehicles (UAVs), commonly known as drones, have witnessed significant advancements in various applications [1–3]. Their increasing affordability, user-friendly operation, and integration of artificial intelligent technologies have prompted a significant shift in diverse fields, from agriculture and environmental monitoring to infrastructure inspection and construction [4–6]. UAVs have had a significant impact on landslide research, especially in on-site surveys, leading to a surge in geoscience publications reliant on UAV-based remote sensing [7,8].

Landslides, characterized by the flow of rock, earth, or debris down slopes [9,10], can be triggered by various external factors, including intense rainfall [11–14], fluctuating water levels [15–18], stream erosion [19,20], changes in groundwater [21,22], earthquakes [23–26], and volcanic activity [27]. Annually, these natural hazards result in extensive property damage, incurring substantial direct and indirect costs [7,28].

A diverse array of geoscience methods has emerged, providing various ways to collect data for a comprehensive understanding of landslides. Surface data on landslides, directly reflecting geomorphological features such as slope angle and displacement, have become an effective method for hazard assessment strategies [29]. These data can be provided by remote sensing methods with high spatial resolution in comparison with ground-based instruments. Manned aircraft and satellites have proven effective in disaster response across a range of temporal and spatial resolutions, covering scales from meters to kilometers. However, utilizing methods like spaceborne photogrammetry and spaceborne Interferometric Synthetic Aperture Radar (InSAR), satellite remote sensing faces issues related to timely data acquisition and atmospheric conditions [30–33]. Airborne remote sensing has

been used for many years, generally based on manned aircraft, which is expensive and inconvenient [34]. Researchers are exploring the use of manned-control UAVs for sensing or photogrammetry of landslide surfaces or beyond surface data, which is flexible, low-cost, and effective compared to manned-aircraft-based sensing [35]. However, the constraints of within-the-horizon flight have limited these UAVs' usage in some applications like emergency response, where flight planning is required. In the past decade, with IMU sensor minimization, autopilot control development, and image processing technology, UAVs equipped with advanced sensors have rapidly emerged as useful tools in landslide analysis, offering cost-effective over-the-horizon flight and a timely method to study landslides. Recent publications about on-site landslide studies suggest that UAVs have become almost a necessary tool to support investigations [7,8].

UAVs have predominantly found application in landslide studies for the monitoring of displacements and the characterization of structures, addressing both the dynamic and static facets of landslides. Leveraged extensively for the static characterization of precarious regions using aerial images [36], UAVs offer a rapid response option in the aftermath of hazard events, particularly when ground investigations are time-consuming. They are also useful in high-resolution 3D model reconstruction based on a number of overlapped aerial images, as UAVs can be closer to landslides to achieve higher spatial resolution compared to spaceborne or airborne remote sensing [37]. Furthermore, the difference between multi-temporal landslide models provides an effective and direct method for short-long term monitoring [38]. In emergency response scenarios, multi-functional UAVs' rapid deployment and data acquisition capabilities aid in post-landslide assessments, enabling real-time monitoring to gauge damage extent, evaluate risks, and inform timely decision making in emergency situations [39–41]. Additionally, as UAV platforms and diverse sensors evolve, applications in landslides, including object identification and real-time change detection, benefit from advanced data analysis techniques in computer vision and machine learning. This enhancement allows for more sophisticated automated analysis of UAV data [42,43].

This article conducts a thorough review of the literature, examining how UAVs contribute to landslide studies and providing an updated look at the technology, covering sensors to data processing. We hope this review can offer the geoscience community a practical update, pointing out potential research areas and addressing associated challenges. Within this paper, we begin by exploring various types of UAVs, sensors, and methods for use in landslide studies. We then present the diverse applications of UAVs in landslide research across three key aspects. The first section discusses their significance in landslide characterization, mapping, and modeling. The following section focuses on monitoring temporal and spatial dynamics in landslide processes, including surface change monitoring to crack and fissure detection. The final section examines the applications of UAVs in emergency response, highlighting effective strategies and the integration of automated detection and machine learning algorithms. To conclude, we underscore the existing challenges, opportunities, and potential future directions within the field.

2. UAVs Description

2.1. UAVs Types

UAVs encompass a diverse array of specifications, with the capability to operate at altitudes ranging from a few meters to several kilometers and carrying weights varying from a few grams to several hundred kilograms. In the realm of landslide studies, UAVs serve various purposes and can be classified based on their aerodynamic and physical features. These classifications include rotary-wing configurations, including helicopters, coaxial designs, quadcopters, and multi-rotors [44]; and fixed-wing designs, encompassing gliders or flying wing models [45]. Notably, the application of helicopters in geoscience studies has swiftly given way to more commercially practical multi-rotors. Fixed-wing UAVs stand out in large-scale surveys and mapping for landslides, adeptly covering extensive areas in a single flight. These drones are most effective in flat or gently sloping

terrains, with their performance potentially limited in comparison to multirotor drones when operating in complex or rugged landscapes. Multirotor UAVs, exemplified by quadcopters or hexacopters, provide versatility for conducting detailed surveys, facilitating close inspections, and monitoring various landslide features. Another emerging category is hybrid drones [46], which combine features of fixed-wing and rotary-wing designs, showing promise in landslide studies. Figure 1 illustrates the features and limitations of each UAV type.

Fixed-Wing	Rotary-Wing		Hybrid-Wing
	Helicopter	Multicopter	
<p>Pros: Efficient coverage for large areas, longer flight endurance;</p> <p>Cons: Cannot hover; cannot maintain above ground level (AGL); require open area for take-off and landing.</p>  <p>CropCam (Air speed ~60km/h, Flying weight 2.7kg, Maximum flying time >30min)</p>	<p>Pros: High efficiency, capable of hovering and close-range inspections;</p> <p>Cons: Mechanically complex</p>  <p>Vapor 55 (Air speed 0--54 km/h, Payload weight <10kg, Maximum hover time 45min)</p>	<p>Pros: Maneuverability, user-friendly;</p> <p>Cons: Limited flight time, less efficient for extensive area coverage.</p>  <p>DJI Phantom 4 (Air speed 0--58 km/h, Flying weight 1.4kg, Maximum hover time 25min)</p>	<p>Pros: Combines vertical takeoff/landing (VTOL) with fixed-wing efficiency, adaptable to various terrains;</p> <p>Cons: Complexity in design and operation, potentially higher cost.</p>  <p>JOUAV CW-15 (Air speed 0--61 km/h, Payload weight <3kg, Maximum hover time 180min)</p>

Figure 1. Functions and limitations on different UAV types.

2.2. Overview of UAV Sensors

Rapid technological advancements in both passive and active sensors have significantly bolstered the capabilities of UAVs across various mission types. Sensors seamlessly integrated into UAVs facilitate image capture at centimeter-scale spatial resolutions and provide temporal resolution conducive to time-dependent analyses. The selection of sensors for a UAV is contingent upon platform size and specific mission objectives. It is worth noting that despite the miniaturization of sensors for UAVs, they often fall short of the capabilities of their ground-based counterparts due to size, power, and environmental constraints. In landslide studies, commonly utilized on-board sensors comprise RGB cameras [44], multi-spectral sensors [47], thermal Infrared Range (IR) cameras [48,49], Synthetic Aperture Radar (SAR) [50–52], and Light Detection and Ranging (LiDAR) [38,53]. Additionally, sensors like electromagnetism and multi-gas find application in specific landslide scenarios.

2.2.1. Optical Sensors

Optical sensors cover the visible (380 nm to 760 nm), near-infrared (760 nm to 1400 nm), shortwave infrared (1400 nm to 3000 nm), and mid-infrared (3000 nm to 35,000 nm) domains. Imagery captured by optical sensors serves as a robust method for landslide analysis, proving particularly effective when visible or thermal effects are prominent. This technique plays a crucial role in efficiently identifying key features, utilizing either human expertise or automated detection approaches in landslide studies. Optical sensors integrated into UAV platforms are commonly classified into visible cameras [54–56], thermal infrared range (IR) cameras [48,49,57,58], and multi-spectral sensors [47,59].

Visible Camera

Visible cameras operate by capturing reflected sunlight and measuring the intensity of light in the visible spectrum. RGB cameras distinguish between red, green, and blue wavelengths, providing valuable color information. These cameras play a pivotal role in landslide detection and mapping by capturing images that emphasize morphological characteristics such as scarps, cracks, the main body, rotated blocks, toes, armchair-shaped

boundaries and river damming. In many existing landslide applications, reliance on RGB camera-based products like orthophotos and DEMs is prevalent due to their effectiveness, directionality and practical implementation. However, it is important to note that visible cameras have limitations, such as being restricted to daylight conditions and susceptibility to adverse weather factors to consider for continuous monitoring. The quality of RGB images, vital for feature identification, depends on various factors, including light source, setting parameters, camera selection, lens distortion, focal length, pixel size, and more [60].

Thermal Infrared Range (IR) Camera

Thermal Infrared Range (IR) cameras operate based on detecting emitted thermal radiation, where warmer surfaces emit more infrared radiation than cooler ones [61]. These cameras determine kinetic temperature and emissivity through intensity, capturing emitted infrared radiation—a phenomenon exhibited by all materials above absolute zero. When mounted on UAVs, thermal infrared range (IR) cameras excel in identifying thermal anomalies associated with geological instability on landslide surfaces. This capability to discern temperature variations offers a unique perspective, enhancing the overall understanding of landslide dynamics. To better localize thermal features, the view field of a thermal camera is designed to be close to that of a normal visible camera. However, it is important to note that thermal images typically have lower spatial resolution than RGB images due to the nature of infrared wavelengths. These cameras may face challenges in certain environmental conditions, such as thick vegetation cover, which can hinder the detection of thermal anomalies. Additionally, the interpretation of thermal data requires careful consideration, as factors like surface moisture and atmospheric conditions can influence temperature readings.

Multi-Spectral Sensors Camera

Multi-spectral sensors function by capturing information across various bands of the electromagnetic spectrum, extending beyond the capabilities of human vision. These sensors can record data at numerous spectral bands, each corresponding to specific wavelengths. In contrast to RGB cameras, which capture three bands, multi-spectral sensors enable a detailed spectral analysis of the terrain, identifying unique signatures associated with geological materials and vegetation information [62]. For instance, the red-edge and near-infrared bands can be highly sensitive to vegetation. This comprehensive spectral information enhances geological mapping and allows for advanced analyses, including assessments of vegetation and mineral identification—crucial aspects in landslide studies. Some UAV-based multi-spectral products are designed to support studies on vegetation detection and analysis, soil moisture estimation, and agriculture. For instance, the Phantom 4 Multi-spectral UAV incorporates a lightweight multi-spectral imaging sensor that yields valuable data in various bands, encompassing the visible, near-infrared, and shortwave infrared domains. This data can be utilized to derive vegetation indices (VIs), including the Normalized Difference Vegetation Index (NDVI) [63]. However, it is worth noting that these sensors often come with trade-offs, such as lower spatial resolution compared to traditional RGB cameras, more complex data processing requirements, and a higher cost.

2.2.2. Light Detection and Ranging (LiDAR)

LiDAR sensors are renowned for their precision in geometric data acquisition [64]. Functioning within the wavelength range of 1000–1600 nm, a LiDAR sensor emits laser pulses directed toward the ground. The sensor records the backscattered signals from various objects such as man-made structures, vegetation, and the ground surface. The returned light energy is then captured by the sensor, and the time taken for the return pulse to travel is employed to calculate the distance covered. The measurements of distance and orientation are accomplished through positioning systems, comprising a positioning system and an inertial measurement unit (IMU), yielding a set of three-dimensional (3D) Cartesian coordinates—X, Y, Z. LiDAR systems can detect multiple echo peaks from various

reflectors, such as the ground or vegetation, allowing for precise measurements of distances to different surfaces. With the miniaturization of LiDAR devices and the increased payload capacity of UAVs, UAV-based LiDAR studies have become more prevalent. UAV-based LiDAR systems offer significant advantages for landslide studies compared to other sensing technologies, including high precision, rapid data collection, and the ability to create detailed 3D models. However, LiDAR does present certain limitations, including susceptibility to atmospheric factors like fog, rain, and sandstorms, as well as interference from dust. These conditions can scatter the laser beam and lead to power attenuation, posing challenges in obtaining precise information about the target [65]. In situations demanding swift responses, such as emergency rescue operations, adverse weather conditions may impede the effective use of LiDAR. Currently, some commercial UAV-based LiDAR systems are reported to be user-friendly and promising in the landslide field like DJI L2, Feima D200.

2.2.3. Synthetic Aperture Radar (SAR)

SAR technology, a remote sensing method employing radar, produces high-resolution Earth surface images that remain unaffected by weather conditions or time of day. Its extensive application spans space-borne, airborne and ground-based platforms, delivering detailed radar images. The process involves emitting radar signals, capturing reflections from the terrain, and processing the data for image generation. Additionally, SAR data supports interferometry, specifically InSAR, utilizing phase information to measure the sensor-to-target distance. This feature allows for the accurate monitoring of land surface changes with precision reaching the centimeter level in landslide studies [66,67]. However, the precision of UAV-based InSAR methods relies heavily on the path accuracy of the flight platform, demanding precision autopilot controls for a repeatable path compared to UAV photogrammetry. GNSS/IMU sensors in UAV platforms are often inaccurate relative to sensor resolution, and UAV platforms are less stable during flight. Despite these challenges, high-altitude UAV SAR systems have been reported [50], benefiting from relaxed absolute path accuracy requirements at greater heights. Various advanced UAV localization technologies, such as real-time kinematic (RTK), vision, and advanced SLAM algorithms [68–72], might address these issues. On the other hand, the complexity of SAR data processing requires specialized knowledge and advanced computational resources. Additionally, SAR systems may face challenges in layover, foreshortening, and shadowing effects [73]. Therefore, the UAV SAR systems currently lack the widespread accessibility of UAV-based photogrammetric mapping systems. Despite this, UAV SAR systems show significant advantages, including the ability to operate in adverse weather conditions, rapid data collection, and detailed 3D modeling, especially when oblique viewing angles are crucial [51,52,74]. The potential for the use of small-size SAR sensors is still very promising, given their development in sensor design and application in landslides, where low-cost multi-rotor UAVs could serve as a viable platform.

In summary, the integration of sensors, including optical, LiDAR and SAR, into UAV platforms enhances the versatility and effectiveness of landslide studies. These sensors provide valuable data for both qualitative and quantitative analyses, making substantial contributions to the field of landslide studies. The functions and limitations of each sensor are presented in Figure 2.

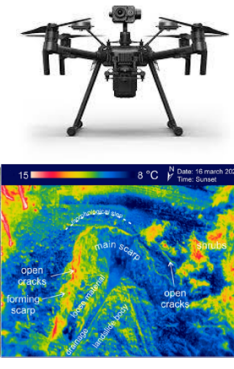
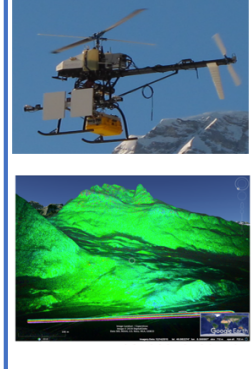
RGB-camera	Multi-spectral camera	IR-camera	SAR	LiDAR
<p>Function: Captures visible light, providing high-resolution color imagery;</p> <p>Limitations: Limited to day light conditions</p> 	<p>Function: Captures data across multiple spectral bands, aiding vegetation identification and classification;</p> <p>Limitations: Might limited spatial resolution</p> 	<p>Function: Detects infrared radiation for identifying temperature;</p> <p>Limitations: Cannot detect geological feature directly; Might limited spatial resolution</p> 	<p>Function: Penetrates through clouds and darkness, providing all weather and day/night monitoring.</p> <p>Limitations: Lower spatial resolution, complex data processing</p> 	<p>Function: Measures distance using laserpulses creating 3D terrain model directly.</p> <p>Limitations: Can be affected by atmospheric conditions, cost</p> 

Figure 2. Functions and limitations of on-board sensors.

3. Integrated UAV Methodology for Landslide Analysis

UAV-based remote sensing in landslide applications typically emphasizes both static characteristic identification and multi-temporal monitoring. Basic static characteristics are derived from mono-temporal aerial images. Subsequently, a static 3D model can be reconstructed based on a series of overlapping aerial images or LiDAR data, providing detailed insights into the topography in three dimensions. Additionally, the differences observed in multi-temporal models serve as a valuable means to monitor the dynamic changes within landslide-prone areas.

3.1. UAV-Based Aerial Images

One of the key advantages of UAVs is their ability to provide bird’s-eye-view images of landslides, a widely-applied function in landslide characterization. The aerial images, captured by optical sensors, play an important role in detecting and mapping landslides based on morphological characteristics such as scarps. Landslide geological surveys often utilize a set of RGB aerial images for landslide static characterization and secondary risk assessment [75,76].

As high-resolution optical sensors continue to advance, UAVs can effectively capture numerous images with high spatial resolution, characterized by the ground sampling distance (GSD). The GSD, usually measured in centimeters per pixel (cm/pixel), denotes the distance between the centers of two adjacent pixels on the ground. This parameter is determined by the simplified function:

$$GSD = \frac{P \times H}{f \times \sin(\theta)}$$

In this equation, H represents the UAV’s height (m), θ is the camera’s pitch angle, P is the pixel size of the sensor (micrometers), and f is the focal length (mm). A larger GSD value indicates lower spatial resolution and decreased visibility of details in the image. For example, considering a DJI Mavic 2 Pro with a focal length of 24 mm (35 mm format

equivalent) flying at a height of 60 m, the GSD would be approximately 1.53 cm/pixel. However, in landslide studies, the situation becomes more complex due to variations in altitude within the field of view, different pitch angles of UAVs and considerations of above-ground level (AGL) fluctuation, which cannot be overlooked in certain cases. The photogrammetric software is instrumental in estimating the averaged Ground Sampling Distance (GSD) of the orthomosaic. This calculation involves determining the average distance from the cameras to the sparse cloud points.

3.2. Model Reconstructions

The limitation of 2D aerial images makes it challenging to distinguish some unstable 3D features, such as near-vertical scarps. Furthermore, a set of aerial pictures with overlap taken by UAVs can be employed for three-dimensional model reconstruction, facilitating more accurate identification of static features in landslides. Commonly used 3D models for landslides include Digital Elevation Models (DEMs), which consist of Digital Surface Models (DSMs) and Digital Terrain Models (DTMs). A Digital Terrain Model (DTM) represents the bare earth surface without any objects, while a Digital Surface Model (DSM) includes the earth's surface with objects. Obtaining these models in the format of point cloud, regular grid or triangular irregulars mesh achievable through technologies like LiDAR [77–79] and stereo photogrammetry using UAVs' optical cameras [37].

3.2.1. UAV-Lidar-Based Reconstructions

Lidar systems are recognized for their reliability in directly outputting three-dimensional coordinates in point cloud format. This precision or UAV-Lidar depends on the accurate localization provided by the platform's Inertial Measurement Unit (IMU) and Global Navigation Satellite System (GNSS) sensors. Measuring the time each pulse takes to return enables precise calculations of distances, and the integration of visible cameras ensures color information in the resulting point cloud. Multiple echo peaks from diverse reflectors, such as the ground or vegetation, contribute to distance measurements. When processing only the last pulses (considered ground echoes), the result is a Digital Terrain Model (DTM), providing a representation of the bare earth surface [64]. The inherent accuracy and direct 3D point clouds output make Lidar a valuable tool for applications in landslide studies.

3.2.2. UAV-Image-Based Reconstructions

High-resolution Digital Elevation Models (DEMs) are increasingly prevalent with the utilization of Structure from Motion (SfM) software and consumer-grade cameras mounted on UAVs. This innovative approach integrates SfM and multiview-stereo (MVS) algorithms, which is different from traditional photogrammetry techniques by requiring minimal expertise and control measurements, along with automated processing. SfM, a computer vision technique, concurrently retrieves 3D camera motion and 3D scene structure from tracked 2D features on overlapping images [80]. Employing images captured by UAVs, this method generates a three-dimensional point cloud, rivaling or even surpassing the quality and resolution of a LiDAR-generated point cloud [81,82].

As shown in Figure 3, the UAV-SfM workflow requires flight planning, considering essential factors like GSD to ensure optimal image resolution and maintaining an image overlap of 60% to 80% for comprehensive coverage. These parameters can be set in some flight planning software [37]. Additionally, in terms of georeferencing, Ground Control Points (GCPs) with known locations are strategically captured to significantly enhance the accuracy of the final 3D model [83–87]. Then, the UAV equipped with a camera captures multiple images from varying angles where the camera orientation can be nadir or oblique. These images, along with GCPs if captured, undergo photogrammetric processing. The software first extracts features like corners and edges from each image and subsequently matches these features across images through camera triangulation. This process calculates the relative positions and orientations of the cameras. Following camera triangulation, the software conducts dense image matching by comparing every pixel in each image to

identify matches. This results in a dense point cloud, portraying the 3D structure of the imaged terrain or object.

The accuracy of the final DEM hinges on various factors influencing the initial image acquisition, with an important element being the GSD, which represents the spatial resolution of UAV images and is intricately linked to factors such as flight height, path, sensor size and landforms. Additionally, model accuracy is contingent on considerations like camera pitch, image overlap, flight trajectory, camera calibration method, and the choice of reconstruction software. Standard approaches for increasing the accuracy of DEMs from UAV data involve the incorporation of direct georeferencing or indirect georeferencing. Direct georeferencing relies on the measured position and orientation of the UAV camera. It is therefore essential to enhance the UAV platform's position accuracy, such as GNSS/RTK or advanced IMU. Indirect georeferencing based on GCPs can be acquired using GNSS/RTK or a total station survey at most sites. Incorporating checkpoints in the validation process serves to assess the precision of the DEM, typically quantified through metrics like Root Mean Square Error (RMSE).

Several investigations have focused on evaluating the accuracy of the UAV-SfM approach. These studies have undertaken a comparative analysis of various SfM software packages, including Agisoft Photoscan, MicMac, and Pix4D Mapper [88–90]. Ouédraogo et al. (2014) [88] compared a Digital Terrain Model (DTM) derived from TLS with those obtained using SfM software (MicMac and Photoscan). James et al. (2012) [90] compared a series of SfM-MVS models with laser scanning, demonstrating that the method is limited by the straightforward camera calibration model used in the software but generally exceeds 1:1000. However, areas without GCPs may still result in locally highly inaccurate DSMs. Liao et al. (2021) [78] conducted a comparison between point clouds generated from UAV-SfM and Lidar across three distinct land cover types, as illustrated in Figure 4. Szypuła et al. (2022) [87] attempted reconstruction without GCPs, which was proven to be unacceptable in some detailed studies like change detection. Overall, the UAV-SfM approach offers a cost-effective and efficient alternative for generating detailed topographic information without the need for extensive ground-based equipment and complex survey setups [91]. SfM-MVS models can be comparable with LiDAR under well-setting flight conditions and with enough GCPs, as well as necessary checkpoints used to evaluate the accuracy of reconstructions.

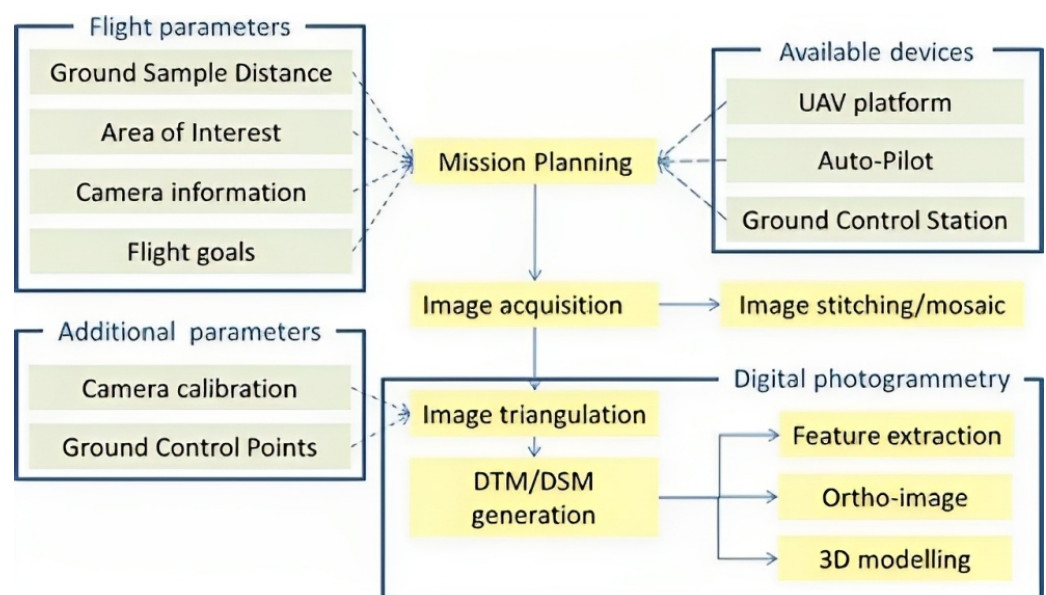


Figure 3. Typical acquisition and processing workflow for UAV images [37].

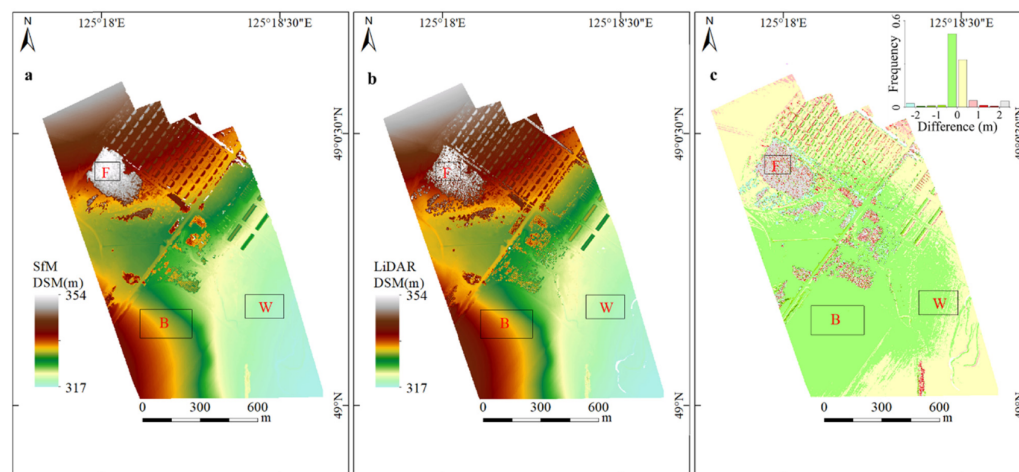


Figure 4. Reconstructions of the study area, including locations of the three subplots: forest (F), wasteland (W), and bare land (B). (a) SfM point cloud, (b) LiDAR point cloud (c) DEM difference calculated by subtracting the LiDAR DEM from the SfM DEM [78].

3.3. Change Detection Based on Multi-Temporal 3D Models

Moreover, it is natural to attempt differentiation of high-resolution DEMs models in time series to detect changes in landslides. Landslide morphology encompasses distinctive surface elements, such as cliffs, source areas, circulation areas, and accumulation areas. Monitoring the displacement of these morphological features is crucial for understanding landslide behavior and assessing potential hazards. A widely employed method for displacement monitoring relies on high-resolution DEMs, often represented as point clouds or mesh models [44,92–95]. Figure 5 offers a comparative overview of common change detection methods, including Differencing of DEMs (DoD), where vertical distances are computed [96]. This pixel-by-pixel differentiation of two DEMs in a time series quantifies vertical changes in the landscape but has inherent limitations in capturing complex three-dimensional displacements. Some methods, such as cloud-to-cloud (C2C) distances using the closest point distance [97] and cloud-to-mesh (C2M) distances computed along the local normal of the mesh [98], offer nuanced perspectives on landscape alterations. However, these methods are constrained by their sensitivity to outliers and may struggle with accurately capturing intricate changes in complex terrains, as their effectiveness depends on factors such as data density and terrain complexity, limiting their applicability in certain scenarios. In contrast, the Multiscale Model-to-Model Cloud Comparison (M3C2) method, computed along a cylindrical axis [99], has emerged as a promising alternative. M3C2 overcomes some of the limitations of traditional methods by providing a mean distance along the normal direction, enabling more accurate and comprehensive monitoring of landscape changes. This method, embedded in some open-source or commercial software such as CloudCompare, has gained popularity for its enhanced capability to capture complex three-dimensional displacements, making it a preferred choice in contemporary UAV-based landslide studies. Moreover, some improved approaches were also proposed to monitor displacement on landslides [100,101].

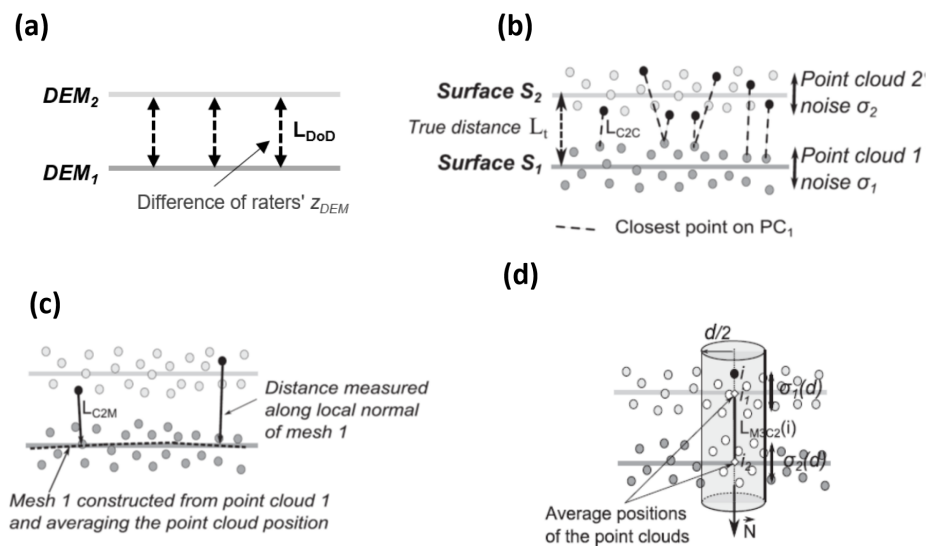


Figure 5. Comparison of common displacement measurement methods between two DEMs including (a) differencing of DEMs (DoD), (b) cloud-to-cloud (C2C), (c) cloud-to-mesh (C2M), and (d) Multiscale Model-to-Model Cloud Comparison (M3C2) [29,99,102].

4. Applications of UAVs in Landslide

UAV applications in landslide studies include three key aspects: geological survey, dynamic monitoring, and emergency response. The static geological survey involves characterizing landscapes through images or 3D models, vegetation investigation and comprehensive landslide mapping and modeling. Dynamic monitoring focuses on volume estimation using multi-temporal differences, surface change detection and monitoring changes in cracks and fissures. When it comes to emergency response, UAVs play a crucial role within a couple of weeks after an event, contributing to search and rescue operations and employing automated detection and machine learning algorithms with UAV-based data.

4.1. Applications of UAVs in Landslide Geological Survey

Timely and accurate landslide surveys are essential for hazard assessment, prediction and effective decision-making strategies. For instance, individuals residing in areas on ancient landslides face potential reactivation risks, posing significant safety concerns. Traditional methods for landslide investigation involve on-site investigations, satellite or airborne imagery, ground surveys using GNSS stations and Lidar-based sensing. Taking into account factors such as efficiency, cost and flexibility, UAVs offer a viable solution for landslide geological survey. The comprehensive geological survey of landslides typically encompasses characterization, mapping and modeling. This section provides the UAV applications on UAV-based geological surveys—a critical aspect for preventing and assessing hazards.

4.1.1. Landslide Mapping and Characterization

Landslide mapping involves the identification and delineation of areas susceptible to landslides, employing geospatial technologies for assessing susceptibility, hazards, and risks. This process is integral to quantitative risk assessment, secondary hazard prediction, and post-disaster reconstruction planning, essential into the stability of environmentally sensitive regions. Traditional approaches to large-scale landslide mapping often rely on the interpretation of spaceborne and aerial photographs from satellites, airplanes, and on-site survey inspections, but trade off spatial resolution when compared to UAV surveys.

UAVs, with their high-resolution capabilities, have proven instrumental in characterizing various landslide features, including scarps, textures, fissures and micro-landforms.

Al-Rawabdeh et al. (2016) [103] employed UAV-derived data for automated landslide scarp recognition, showcasing the effectiveness of image-based analysis algorithms in distinguishing landslide scarps (Figure 6). Characterization of landslides serves as a fundamental step for a thorough exploration of landslide dynamics. In 2018, Peng et al. [104] utilized UAV-captured aerial images to identify 69 landslides around Heifangtai (Yongjing, China). Their study highlighted the surface deformation direction of slopes and the bedding dip angle of bedrock as influential factors. Additionally, Qiu et al. (2018) [105] conducted field investigations supplemented by UAV images, pinpointing 275 landslides in Zhidan County, China. Their research explored the effects of slope length and gradient on the size distributions of the characterized landslides.

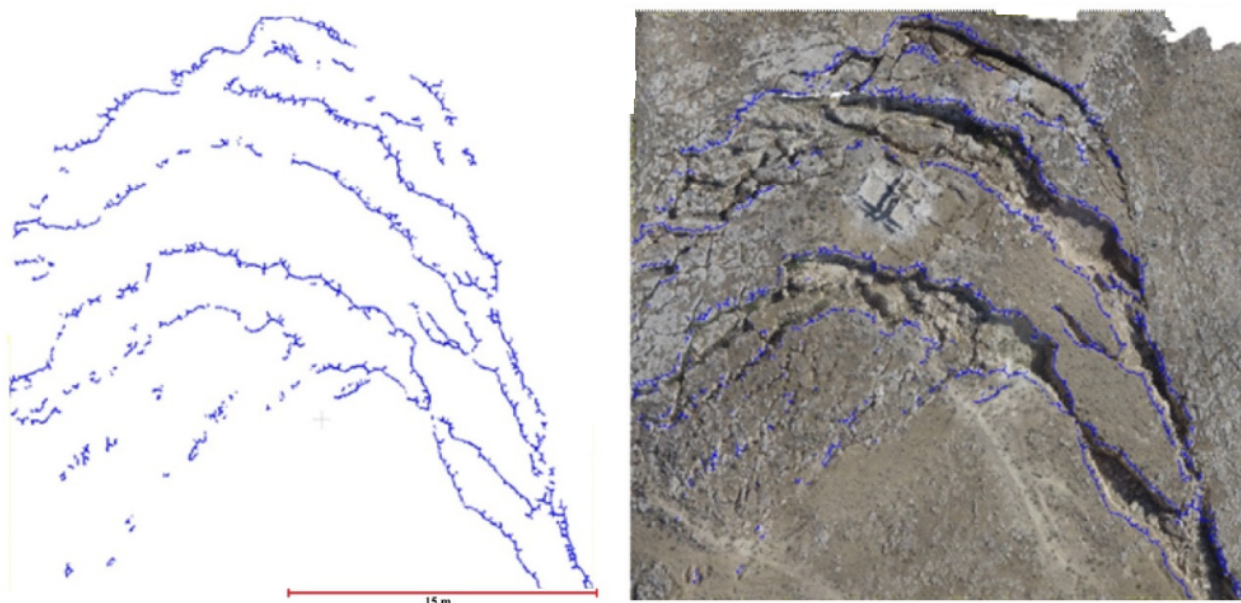


Figure 6. Landslide scarp detection results (blue) overlaid on the orthophoto captured by UAV of study area [103].

4.1.2. Landslide Model Reconstruction

Digital models, offering comprehensive information about landslides, are gaining popularity in risk management and geoscience information systems due to their accuracy and flexibility. Commonly employed digital model reconstructions for landslides include digital orthophoto maps (DOMs) and digital elevation models (DEMs). DOMs result from the amalgamation of images captured by UAVs, providing detailed geological information such as the length, width and geometry of landslides, with high spatial resolution to capture localized surface details. However, they lack height information. On the other hand, DEMs, which can be attached with height data include (DSMs) or exclude (DTMs) natural and man-made objects located on the landslide.

For instance, Colica et al. [55] reconstructed a model using UAV photogrammetry to survey a landslide in northern Malta, emphasizing the importance of digital geological surveys. High-resolution DEMs can also serve as a fundamental layer in GIS systems, providing valuable information. Hu et al. [106] analyzed the digital terrain topographic features of a landslide using a high-resolution DEM obtained by UAV-SfM, reflecting the risk area. Moreover, DEM models obtained by UAVs can be input geometry in numerical simulation [107–110]. Ouyang et al. (2019) [110] explored the use of UAV-based high-resolution DEMs to capture the initial deformation of large sequential landslides, demonstrating their potential as input geometry in numerical simulations for evaluating potentially landslide-prone areas. Lin et al. (2021) [111] investigated geological structures using UAV Lidar, inputting the data into the failure mechanism simulation of the landslide. Table A1 provides a summary of recent applications of UAV-based Model Reconstruction.

4.1.3. Landslide Susceptibility Mapping

Landslide susceptibility, influenced by morphometric and hydrological terrain conditions, signifies the probability of landslide occurrences driven by geodynamic processes and represents geohazard [112]. The assessment of landslide susceptibility is essential for the implementation of preventive measures in areas prone to landslides, providing vital information for concerned agencies [113,114]. Geospatial studies commonly leverage remote sensing data through Geographic Information System (GIS) platforms, employing integrated decision models to formulate comprehensive landslide susceptibility maps. These models incorporate various parameters, such as the topographic wetness index, slope (angle, gradient, aspect) index (SI), normalized difference vegetation index (NDVI), stream power index (SPI), etc. UAV-based sensing contributes detailed DEMs data, including the slope index (SI) [115]. UAV sensing also provides advantages for NDVI, a parameter indicating the vegetation density of an area. NDVI, derived from the normalized ratio of Near-Infrared (NIR) to red band reflectance, enables the monitoring of green vegetation density and health [116]. Bhatt et al. (2013) [117] observed that regions with dense forest coverage show decreased susceptibility to landslides, while Song et al. (2012) [118] highlighted the role of tree roots in slope stability and soil moisture reduction. As a result, the NDVI is considered an essential parameter in landslide susceptibility assessments. By combining UAV-based multispectral and visible RGB cameras, NDVI can be calculated as a thematic layer in GIS, supporting the computation of landslide susceptibility. For instance, Gantimurova et al. (2021) [47] demonstrated the calculation of landslide susceptibility based on NDVI and DEMs using UAV-based multispectral and visible RGB cameras. Some other key parameters are also used in landslide susceptibility calculation (Figure 7).

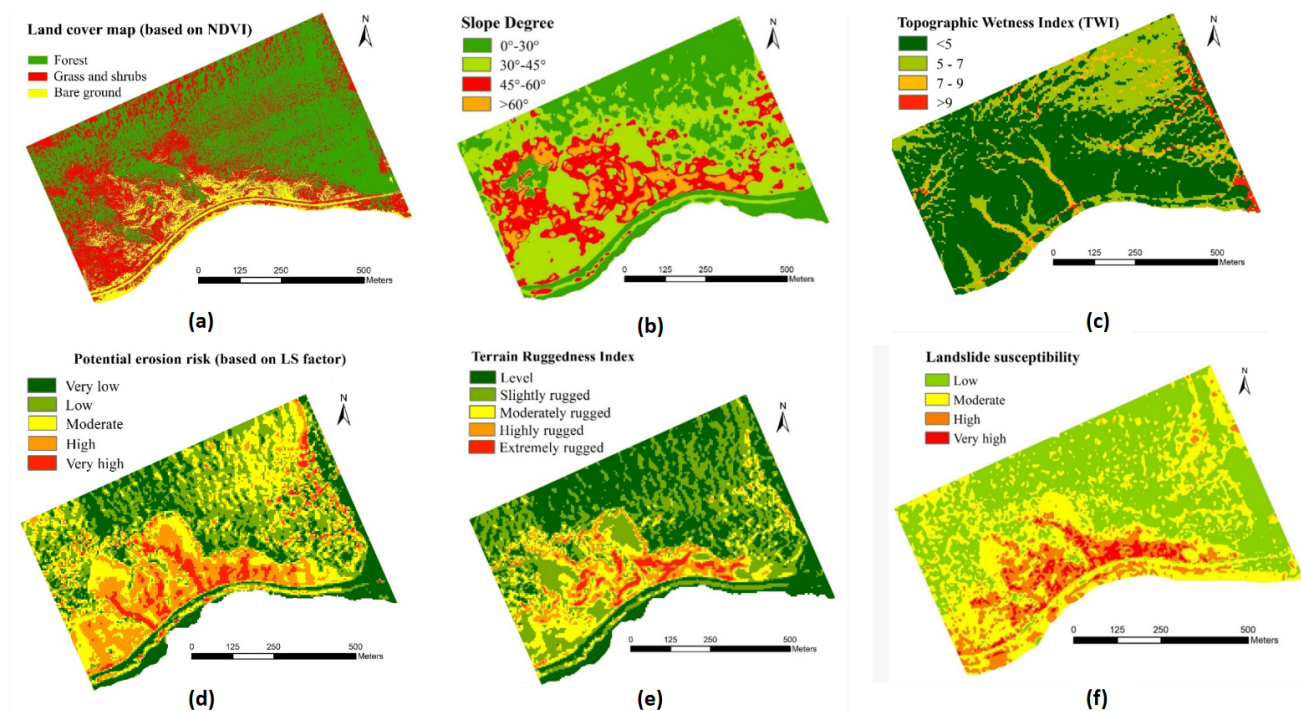


Figure 7. Conditioning factor mapping on DEM: (a) land cover map (based on NDVI); (b) slope angle map (based on DEM); (c) TWI map; (d) LSF map; (e) TRI map; (f) landslide susceptibility map [47].

4.2. UAV Applications for Landslide Monitoring

4.2.1. Surface Change Monitoring with UAV-Based Sensing

Monitoring the dynamic changes in landslides requires both temporal and spatial resolutions to study the evolution and assess risks [42,119]. The surface change of landslide monitoring focuses on whether the landslide moves and how the landslide moves.

UAVs facilitate landslide volume estimation—a critical aspect for assessing the risk of landslides and secondary hazards by providing pre- and post-sliding topographic data that require comparison in multi-temporal settings. Ma et al. (2020) [120] estimated the total volumes of the source zone and accumulation zone of the Zaoling landslide (Xiangning, China) at 77,000 and 82,000 m³, respectively, using high-resolution UAV photogrammetry. For larger coverage fixed-wing UAV surveys, Saito et al. (2018) [45] identified 54 coseismic landslides within the Sensuikyo area (Aso, Japan), with volumes ranging from 9.1 to 3994.6 m³. The application of UAVs for monitoring whether the slope surface moves provides a valuable and efficient alternative, enabling detailed and accurate mapping of landslide features.

Additionally, conventional ground-based sensing techniques, limited to a few monitoring points along unstable slopes [121,122], restrict the understanding of complex and heterogeneous ground motion, as well as the kinematic behaviors of large landslides. Based on change detection methods in Section 3.3, UAVs present several advantages for morphological monitoring of landslides compared to traditional methods. They can capture high-resolution imagery, access challenging terrains, and collect data frequently and at a lower cost [123]. Therefore, the adoption and further development of this technology for time-series landslide monitoring are increasingly popular. For example, Mazzanti et al. (2021) [124] compared UAV SFM-based point clouds and Lidar scanning point clouds using the M3C2 algorithm in which data were obtained six times from 2015 to 2018, showing an active geomorphological evolution of the rock scarp area due to frequent rockfalls and topples. Bentley et al. (2023) [95] detected surface displacement with a 5-year monitoring program based on UAV-based photogrammetry, indicating there were sufficient pre-failure deformations. However, as aerial image acquisition requires time, it might limit the application of this method in some fast-moving landslides.

Besides 3D cloud of DEMs for surface change monitoring of landslides, UAVs can also serve as platforms for SAR, which is particularly valuable in landslide monitoring. UAVSAR often incorporates interferometric synthetic aperture radar (InSAR) techniques, allowing it to analyze changes in the Earth's surface by comparing multiple radar images taken at different times to detect ground deformations and provide crucial information for assessing landslide risk and understanding dynamic geological processes. NASA/JPL deployed an airborne SAR system in an optimal natural laboratory, specifically at the Slumgullion landslide in Colorado, depicted in Figure 8a. This landslide has experienced movement at rates of tens of millimeters per day for centuries [125–127]. Delbridge et al. (2016) [50] present a method for characterizing 3D surface deformation using the UAVSAR system, applied to the Slumgullion Landslide. They demonstrated the accuracy of UAVSAR-derived vector velocity measurements in capturing landslide dynamics, revealing seasonal variations in movement, and employing an inversion framework to determine slide thickness and basal geometry (Figure 8b). However, such applications based on InSAR to monitor surface changes of landslides require precision autopilot controls to enable flying the same path with very high accuracy to ensure the two UAVSAR radar images are from the same location, which can be differenced to show the changes between the images. For smaller size UAVs, Frey et al. (2021) [74] utilized a compact frequency-modulated continuous wave (FMCW) L-band SAR system mounted on Aeroscout's UAV Scout B1-100. They conducted an interferometric repeat-pass SAR data acquisition, achieving high-quality results over diverse natural terrain.

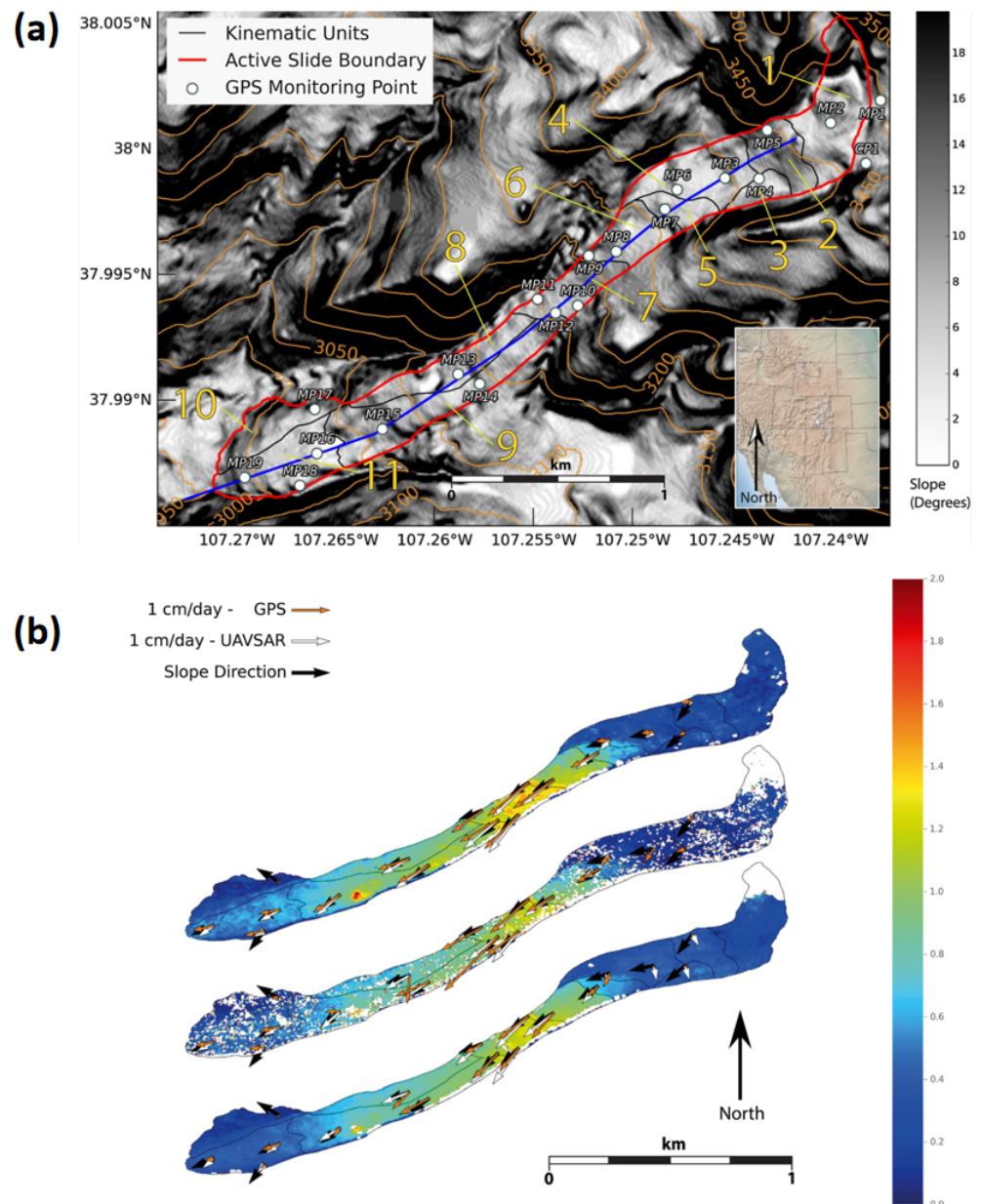


Figure 8. (a) Slope and elevation of the Slumgullion Landslide (11 kinematic units) and surrounding terrain; (b) comparison of GPS- and UAVSAR-derived horizontal velocity vectors [50].

4.2.2. Crack and Fissure Change Monitoring Using UAV-Based Sensing

Within the broader scope of UAV applications in landslide monitoring, one of the crucial aspects is the detection of crack and fissure changes. Understanding the dynamics of cracks in landslide-prone areas is essential for landslide evolution and comprehensive risk assessments [128–130]. Traditional approaches to monitoring changes in cracks predominantly depend on on-site investigations and the use of crackmeters [131,132]. However, advancements in high-resolution remote sensing techniques now enable the monitoring of cracks at landslide sites with the assistance of UAVs.

In fact, an RGB camera can offer high-resolution images where cracks can be detected by visual inspection or some semi- or fully automated detection algorithms [103,133]. For example, Cheng et al. (2021) [54] employed UAV photogrammetry to assess a landslide through detailed field surveys and automatic crack recognition using deep learning. The behavior of the landslide was investigated by comparing the identified cracks on two

different dates after the landslide event. This comparative analysis provided supporting evidence regarding the stability of the landslide. However, RGB images are not always feasible in some cases without a good light source. As any object with a temperature higher than absolute zero emits electromagnetic radiation within the infrared (IR) band, known as “thermal radiation”, an IR thermal camera is a novel operational tool for monitoring cracks on unstable landslides [48,49,57,58]. As shown in Figure 9, Vivaldi et al. (2022) [134] introduces an approach to landslide monitoring using UAV-based infrared thermography. Through the integration of three-dimensional models generated from aerial RGB photogrammetry and thermal outcomes from infrared thermography, the research successfully monitors the state and distribution of landslide activity, detecting features such as forming cracks, scarps, wet terrain portions and loose material. However, it is worth noting that factors such as direct exposure to sunlight, visibility, and a reasonable distance from the landslide should be fully considered before the usage of UAV-based IR sensing [135]. In specific scenarios, such as gas and oil pipeline areas susceptible to landslides, the utilization of UAV-based gas sensing proves invaluable, offering a potential contribution to comprehensive landslide monitoring efforts by providing crucial information into environmental conditions and potential risks [136–139]. This technology enables enhanced surveillance, aiding in the early detection and management of landslide-related challenges in critical infrastructure zones.

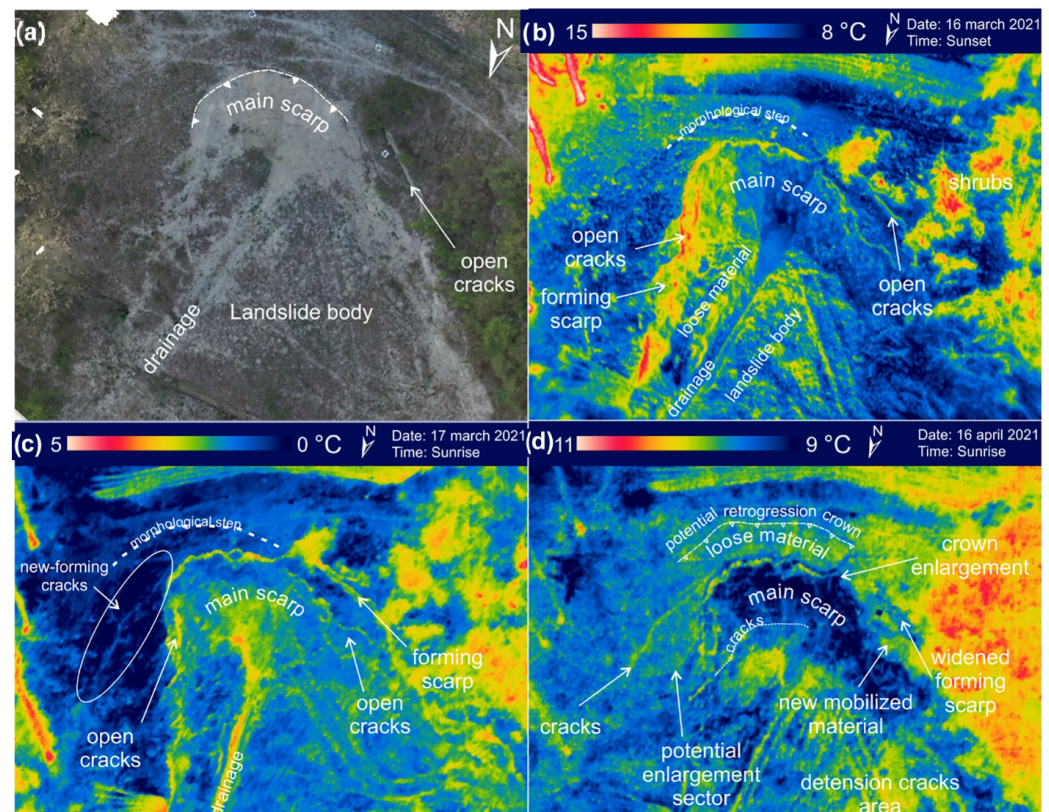


Figure 9. Comparison of Airborne RGB-photogrammetry and infrared thermography applied to landslide remote monitoring. (a) Aerial photo of the area framed by IRT in insets; (b) focus of the landslide depletion zone taken late in the evening on March 2021; (c) focus of the landslide depletion zone taken early in the morning on March 2021; and (d) focus of the landslide depletion zone taken early in the morning on April 2021 [134].

4.3. UAV Applications in Emergency Response

4.3.1. Emergency Response Strategies

According to DJI’s official website, more than 1000 lives have been saved by their UAV products in diverse disaster situations over the last decade [140]. This attests to the pivotal

role that UAVs play as essential tools for emergency rescue operations, safeguarding lives during critical moments. In landslide disasters, UAVs stand out for their easy operation and ability to capture high-resolution images, making them valuable tools for aiding decision-making by local governments [39–41]. When a landslide disaster occurs, attention is immediately drawn to the rescue of survivors, the assessment of landslide activity, and the potential secondary hazards associated with the event [141–143]. Emergency investigation and monitoring in the weeks following such occurrences are crucial, providing insights into the stability of the landslide. Ground-based investigation methods are often limited by challenging weather conditions and difficult-to-reach slope surfaces. Herein, UAV-based remote sensing presents an effective solution, enabling rapid response and comprehensive monitoring.

UAVs swiftly identify unsafe conditions, including growing cracks and scarp areas, by capturing high-resolution imagery and videos. In addition, the UAVs are able to respond to emergent landslides within a couple of days. For instance, as shown in Figure 10, in the aftermath of an earthquake-induced landslide in Sichuan, China, Jiang et al. (2022) [144] utilized UAV photogrammetry-based 3D modeling only one day after the event, combined with ground-based SAR (GB-SAR) and TLS. This approach not only identified the landslide but also provided crucial insights into the failure mechanism, explaining how early slope reinforcement delayed the occurrence by four and a half hours after the earthquake. Similarly, in the case of a rainfall-induced landslide in Zhonghaicun, Sichuan, China, an emergency investigation was promptly conducted after continuous torrential downpours [145]. Utilizing a DJI Phantom 4 Pro UAV, high-resolution orthophotographs, and digital elevation models (DEMs) were obtained for the entire landslide area. Beyond static identification, continuous monitoring in the weeks following the event was imperative for assessing landslide activity. In a 20-day emergency investigation of the ancient Aniangzhai landslide triggered by a short-duration rainstorm and Meilong debris, Zhao et al. (2021) [146] employed daily UAV (DJI Phantom 4 RTK) images. Their findings indicated a reactivation of the ancient landslide, maintaining a constant deformation state with an approximate rate of 5 mm/h.

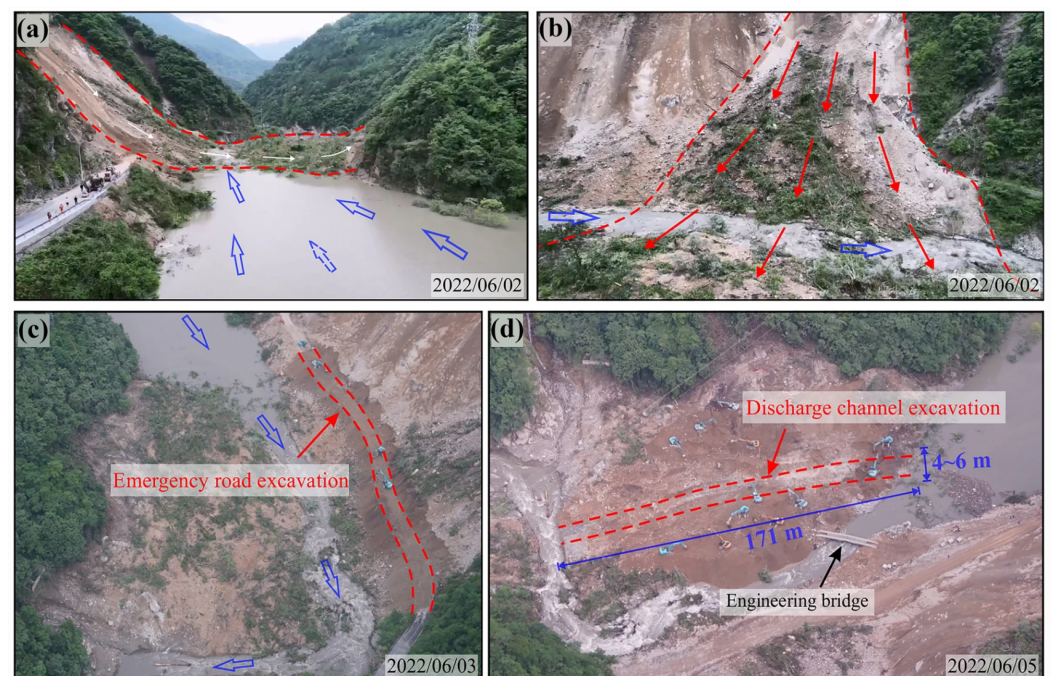


Figure 10. UAV aerial views capturing landslides and a dammed lake since one day after landslide event: (a,b) showcase the preliminary investigation of the landslide dam and the resulting lake; (c) depicts the landslide dam during the emergency road excavation; (d) displays the excavation of the emergency discharge channel at the landslide dam site [144].

Protecting human life stands as one of the paramount goals in the realm of hazard studies, a mission where UAVs play a pivotal and life-saving role, particularly in the field of disaster relief. In disaster scenarios, the urgency to locate and aid survivors is often hindered by the perilous conditions faced by first responders, who themselves grapple with life-threatening risks akin to those confronted by the victims. The past decade has witnessed a notable simplification in UAV operations, notably in aspects such as First Person View (FPV), which enables support for over-the-horizon flight. This simplification has been instrumental in extending the reach of first responders, offering a solution for survivor searches while effectively keeping operators away from hazardous and inaccessible areas. UAVs, equipped with FPV capabilities, enable operators to navigate treacherous terrains with a heightened awareness of their surroundings. This not only expedites the search and rescue process but also minimizes the exposure of operators to potential dangers. Illustrating the life-saving potential of UAVs in landslide disasters, numerous instances exemplify their crucial role in ensuring the safety of both survivors and first responders. In the aftermath of a landslide in the village of Ask, Norway (2020), where emergency personnel were not allowed to try entering any of the collapsed homes because of safety issues, UAVs equipped with FPV and thermal imaging device capabilities swiftly surveyed the area, aiding search and rescue teams in identifying 13 survivors and a missing Dalmatian (Figure 11) [147,148]. Similarly, during a landslide event in Putumayo province, Colombia, UAVs played a critical role in supporting rescue amidst challenging conditions, generating 3D maps and providing critical information for timely and effective emergency response [149]. UAVs' role in disaster relief becomes increasingly important, contributing to the safeguarding of lives and the enhancement of overall emergency response capabilities.

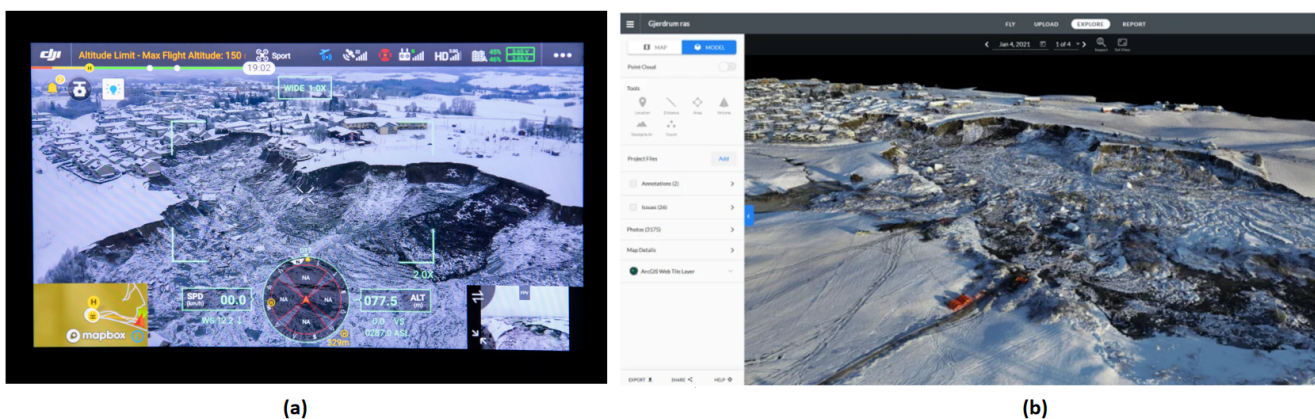


Figure 11. Ask Landslide, December 2020: (a) FPV view of a UAV operator; (b) an interactive 3D model (DEM) of the area [148].

While UAVs prove valuable in emergency response, certain limitations merit consideration. Unfavorable weather conditions, such as heavy rainfall or strong winds, may impede UAV flights, potentially causing delays in critical response efforts and restricting access to disaster-stricken areas. The operational range of UAVs may pose challenges when dealing with remote or geographically isolated locations. Moreover, the endurance and flight time of UAVs are constrained, necessitating careful planning for extended monitoring periods. The requirement for skilled operators and specialized equipment adds complexity, potentially influencing the immediacy of response efforts. Despite these challenges, the remarkable versatility and swift deployment of UAVs emphasize their crucial role in emergency response scenarios. Researchers and practitioners should be aware of these limitations while recognizing the significant potential of UAVs to save lives during emergencies, prompting ongoing exploration and collaboration to enhance UAV technology in disaster response.

4.3.2. Automated Detection and Machine Learning Algorithms Using UAV-Based Data

As Machine Learning and edge computation progress, a new set of tools is emerging, making use of UAV-captured data to automatically detect signatures in dynamic data streams. This capability is particularly valuable in emergency response scenarios [150]. With the swift collection of data, these tools often employ machine learning or edge computation algorithms for efficient feature extraction, ensuring that data analysis keeps pace with the cadence of UAV data collection. This shift represents a transformative field in geomorphic change analyses, facilitating timely and scientifically informed investigations.

Lian et al. (2020) [76] showcased the potential of UAV-based rapid identification by combining DOM and DEM generated from low-altitude UAV aerial images. This method proved highly effective in swiftly and accurately identifying landslides, collapses and cracks. The accuracy of crack identification reached 93%, while landslide and collapse identification achieved 100%. These UAV-based rapid identification methods can also be integrated with other remote sensing methods. For instance, Jiang et al. (2022) [151] proposed a fusion method that integrates TLS and UAV photogrammetry for landslide deformation monitoring, especially in complex terrain conditions. This method uses TLS to augment the number and range of ground control points (GCPs) visible to UAVs, subsequently employing assumed control points (ACPs) to reconstruct the UAV model. The calculated landslide displacement, compared with monitoring data obtained by GNSS, demonstrates reasonable agreement, highlighting the efficacy of this fusion method. Catani (2021) [75] investigates the fusion of UAS-captured images, data from autonomous sources, and non-nadir web-crowd-sourced imagery. The study employs convolutional neural network (CNN) algorithms to assess the viability of non-standard images for automated landslide detection and geomorphic mass movement analysis. While open-source CNN classification schemes prove effective in identifying geomorphic mass movements, the study cautions against directly applying specific CNNs to UAS-captured imagery. It emphasizes the need for a nuanced balance between computational power requirements and analysis speed. Recent contributions by Yun et al. (2023) [152] showcased the application of an Improved Mask R-CNN Model for landslide area detection using UAV images. This advancement yields a noteworthy improvement, achieving a recall of 91.4% and an accuracy of 92.6%, underscoring the potential for enhanced precision in landslide identification. Furthermore, Qi et al. (2022) [43] make significant advancements by combining UAV remote sensing image technology with machine learning, creating a landslide feature extraction system. This system, integrated with experimental design, undergoes rigorous verification to assess its performance. Such integrative approaches signal a promising trajectory in emergent response systems that meld UAV technology and machine learning to refine the understanding and analysis of geomorphic changes.

5. Challenges and Opportunities

The integration of UAVs in geological surveys presents both challenges and promising opportunities for advancing landslide studies. One critical challenge revolves around regulatory frameworks, with some regions imposing restrictions on UAV flight. These regulations, shaped by privacy concerns and airspace management, impact the scope and efficiency of UAV-based surveys. Additionally, the limited hover time of UAVs poses operational challenges, restricting operators from venturing far from landslide-prone areas. This constraint increases the potential risk for personnel involved in emergency response activities post-landslide events. Also, the advancement of UAVs in navigation and control emerges as a key focal point. Moreover, SfM algorithms make 3D reconstruction simple for users and mainstream UAV usage. However, the accuracy of DEMs strongly depends on the setting of Ground Control Points (GCPs) on-site. New approaches, such as the co-alignment method, attempt to make GCPs more effective [153]. In situations where the landslide is accessible, it is crucial to increase 3D reconstruction accuracy without GCPs. Addressing these issues is paramount for optimizing UAV applications in landslide studies.

The utilization of UAV swarms presents a promising avenue, offering enhanced mapping capabilities and improved efficiency, especially in emergency scenarios. Additionally, the life-saving potential of UAVs in geohazard situations is crucial. UAVs, with their rapid deployment capabilities, play a crucial role in emergency response strategies. Future research should focus on enhancing the resilience of UAV systems, exploring swarm technologies, and conducting in-depth studies on their applications in emergency scenarios. By addressing these challenges and capitalizing on emerging opportunities, UAVs stand poised to revolutionize landslide studies and contribute significantly to risk assessment and emergency response efforts. For geoscience research and engineering, it is necessary to pay heightened attention not only to fully commercial technology but also to the rapid advancements in UAV technology. The integration of features such as localization technology, swarm capabilities, and other emerging technologies might stand as a potential revolutionary force.

Overall, UAVs have significantly shaped modern landslide studies, playing a pivotal role in on-site investigations owing to their remarkable attributes, including high spatial resolution, cost-effectiveness, and adaptability. While these qualities contribute to their indispensability, careful consideration of challenges, such as regulatory restrictions, operational limitations, and environmental impact, becomes imperative to ensure the sustainable and efficient application of UAVs in landslide studies.

6. Conclusions

This review of UAV applications underscores their significant contributions in landslide studies across investigation and monitoring. The exploration began by focusing on the identification of static characteristics, elucidating the intricacies of static features such as landslide characterization, mapping, and modeling. This foundational understanding forms the basis for a nuanced comprehension of the geological facets associated with landslides. In terms of change monitoring, UAVs equipped with high-resolution capabilities emerge as crucial assets, offering detailed temporal and spatial data to monitor the evolving nature of landslide processes. We further emphasize the essential role of UAVs in emergent response scenarios post-landslide events, showcasing their effectiveness in immediate response strategies and automated detection through machine learning algorithms. Despite the significant impact of UAVs, the review discussed ongoing challenges, including regulatory hurdles, hover time limitations, SfM accuracy, and the potential integration of advanced technologies like UAV swarms.

In conclusion, this review sheds light on the crucial role of UAVs in landslide studies. The integration of UAV technology not only enhances our understanding of static and dynamic landslide characteristics but also proves instrumental in emergency response efforts. As technological landscapes evolve, embracing new advancements and capitalizing on opportunities will be crucial for the geoscience community to explore and maximize the potential applications of UAVs in landslide research.

Author Contributions: Conceptualization, investigation, writing—original draft preparation, J.S.; writing—review and editing, G.Y., L.S. and H.Z. All authors have read and agreed to the published version of the manuscript.

Funding: This research was supported by the National Natural Science Foundation of China: The Young Scientists Fund (Grant No. 52105537).

Conflicts of Interest: The authors declare no conflicts of interest.

Abbreviations

The following abbreviations are used in this manuscript:

UAV	Unmanned Aerial Vehicle
GNSS	Global Navigation Satellite Systems
TLS	Terrestrial Laser Scanners
InSAR	Interferometric Synthetic Aperture Radar
IR	Infrared Range
LiDAR	Light Detection and Ranging
DOM	Digital Orthophoto Map
DEM	Digital Elevation Model
DSM	Digital Surface Model
DTM	Digital Terrain Model
SfM	Structure-from-Motion
GCP	Ground Control Point
M3C2	Multiscale Model-to-Model Cloud Comparison
RTK	Real-time Kinematic
NDVI	Normalized Difference Vegetation Index
GIS	Geographic Information System

Appendix A

Table A1. Summary of Recent UAV-based DEM Applications in Landslide Studies.

Reference	Scientific Issue, UAV Platform, Camera	Flight Parameter	GSD, Software, Accuracy
Chen et al. (2021) [54]	Landslide modeling; Multicopter-Feima D200; SONY RX1RII with 35.9 × 24 mm sensor	55 m AGL, overlap/sidelap rate: 80%/65%	GSD 0.9 cm/pixel; Feima UAV manager; RMS _{xy} < 1.7 cm, RMS _z < 1.4 cm
Colica et al. (2021) [55]	Geological surveys; Multicopter-DJI Phantom 4 Pro; 1" CMOS, 20-MP RGB camera	30 m above the launch location, overlap/sidelap rate: >80%/>60%	GSD 0.87 cm/pixel; Agisoft Metashape; RMSE = 0.87 cm
Chang et al. (2020) [56]	Geological surveys; Fixed-wing-Skywalker X8; Nikon D800E	1500–3000 m AGL, overlap/sidelap rate: >80%/>60%	GSD 15 cm/pixel; Pix4D Mapper; RMSE = 0.13–0.47 m
Hu et al. (2019) [106]	Landslide modeling; Multicopter-DJI Mavic Pro; 1/2.3" CMOS, 12.35 MP camera	149.7 m above the launch location, overlap/sidelap rate: 75%/75%	GSD 5 cm/pixel; unknown software; RMSE = 0.5 m
Rodriguez-Caballero et al. (2021) [154]	Landslide modeling; Multicopter-DJI Phantom 4; 1" CMOS, 20-MP RGB camera	60 m above the launch location, overlap/sidelap rate: 75%/65%	unknown GSD; Pix4Dmapper; RMS _x = 0.096 m, RMS _y = 0.14 m, RMS _z = 0.33 m
Büschelberger et al. (2021) [155]	Landslide characterization; Multicopter-DJI Mavic Pro; 1/2.3" CMOS, 12.35 MP camera	110 m above the launch location, overlap/sidelap rate: 75%/65%	GSD < 5 cm/pixel; Agisoft Metashape; 1.4 pixels
Vassilakis et al. (2021) [67]	Landslide modeling; Multicopter-DJI Phantom 4; 1" CMOS, 20-MP RGB camera	120 m/140 m above the launch location, overlap/sidelap rate: 75%/65%	GSD unknown; Agisoft; <1 cm

Table A1. Cont.

Reference	Scientific Issue, UAV Platform, Camera	Flight Parameter	GSD, Software, Accuracy
Dille et al. (2020) [156]	Landslide modeling; Multicopter-DJI Phantom 3 Pro; 1/2.3" CMOS camera, 12 MP RGB camera	115 m above the launch location, overlap/sidelap rate: 85%/75%	GSD 5 cm/pixel; Agisoft Photoscan; RMSx = 0.07 m, RMSy = 0.24 m
Koutalakis et al. (2021) [157]	Landslide modeling; Multicopter-DJI Mavic 2 Pro; 1" CMOS, 20-MP RGB camera	50 m above the launch location, overlap/sidelap rate: unknown	GSD unknown; Pix4Dmapper Pro; RMSE = 6 cm
Sandric et al. (2023) [158]	Landslide modeling; Multicopter-DJI Phantom 4; 1" CMOS, 20-MP RGB camera	114 m above the launch location, overlap/sidelap rate: 70%/70%	GSD unknown; ArcGIS Pro (ESRI); RMSx = 0.14–0.23 m, RMSy = 0.12–0.33 m, RMSz = 0.42–0.56 m
Xu et al. (2020) [159]	Landslide modeling; 1: Multicopter-MD4-1000; Sony ILCE-7R camera; 2: Fixed-wing-Feima F1000;	1: 450 m above the launch location, overlap/sidelap rate: 60%/80%; 2: 270 m above the launch location, overlap/sidelap rate: 65%/80%	GSD 1.6 cm/pixel; GSD 2.4 cm/pixel; Pix4D Mapper, Polyworks; 1: RMSx 0.02–0.05 m, RMSy 0.03–0.04 m, RMSz 0.05–0.11 m; 2: RMSx 0.03–0.04 m, RMSy 0.02–0.04 m, RMSz 0.03–0.06 m;
Conforti et al. (2020) [160]	Landslide modeling; Multicopter-Parrot Anafi 21 Mp RGB camera	131 m above the launch location, overlap/sidelap rate: 85%/80%	GSD 6.7 cm/pixel; Pix4D Mapper; RMSx = 0.19 m, RMSy = 0.18 m, RMSz = 0.21 m
Zarate et al. (2023) [161]	Landslide modeling; Multicopter-DJI Phantom 2; GoPro 3+ camera	84.2–89 m above the launch location, overlap/sidelap rate: 70%/70%	GSD 4.0–4.3 cm/pixel; Agisoft PhotoScan; RMSE = 0.01–0.04 m

References

- Floreano, D.; Wood, R.J. Science, technology and the future of small autonomous drones. *Nature* **2015**, *521*, 460–466. [[CrossRef](#)] [[PubMed](#)]
- Song, B.D.; Park, K.; Kim, J. Persistent UAV delivery logistics: MILP formulation and efficient heuristic. *Comput. Ind. Eng.* **2018**, *120*, 418–428. [[CrossRef](#)]
- Otto, A.; Agatz, N.; Campbell, J.; Golden, B.; Pesch, E. Optimization approaches for civil applications of unmanned aerial vehicles (UAVs) or aerial drones: A survey. *Networks* **2018**, *72*, 411–458. [[CrossRef](#)]
- Raj, R.; Kar, S.; Nandan, R.; Jagarlapudi, A. Precision agriculture and unmanned aerial Vehicles (UAVs). *Unmanned Aerial Vehicle: Applications in Agriculture and Environment*; Springer: Berlin/Heidelberg, Germany, 2020; pp. 7–23. [[CrossRef](#)]
- Manfreda, S.; McCabe, M.F.; Miller, P.E.; Lucas, R.; Pajuelo Madrigal, V.; Mallinis, G.; Ben Dor, E.; Helman, D.; Estes, L.; Ciruolo, G.; et al. On the use of unmanned aerial systems for environmental monitoring. *Remote Sens.* **2018**, *10*, 641. [[CrossRef](#)]
- Elghaish, F.; Matarneh, S.; Talebi, S.; Kagioglou, M.; Hosseini, M.R.; Abrishami, S. Toward digitalization in the construction industry with immersive and drones technologies: A critical literature review. *Smart Sustain. Built Environ.* **2021**, *10*, 345–363. [[CrossRef](#)]
- Garnica-Peña, R.J.; Alcántara-Ayala, I. The use of UAVs for landslide disaster risk research and disaster risk management: A literature review. *J. Mt. Sci.* **2021**, *18*, 482–498. [[CrossRef](#)]
- Gomez, C.; Purdie, H. UAV-based photogrammetry and geocomputing for hazards and disaster risk monitoring—A review. *Geoenviron. Disasters* **2016**, *3*, 23. [[CrossRef](#)]
- Cruden, D. A simple definition of a landslide. *Bull. Eng. Geol. Environ.* **1991**, *43*, 27. [[CrossRef](#)]
- Dai, F.C.; Lee, C.F.; Ngai, Y.Y. Landslide risk assessment and management: An overview. *Eng. Geol.* **2002**, *64*, 65–87. [[CrossRef](#)]
- Maturidi, A.M.A.M.; Kasim, N.; Taib, K.A.; Azahar, W.N.A.W. Rainfall-induced landslide thresholds development by considering different rainfall parameters: A Review. *J. Ecol. Eng.* **2021**, *22*, 85–97. [[CrossRef](#)]
- Tohari, A. Study of rainfall-induced landslide: A review. In *Proceedings of the IOP Conference Series: Earth and Environmental Science*; IOP Publishing: Bristol, UK, 2018; Volume 118, p. 012036.

13. Lee, M.L.; Ng, K.Y.; Huang, Y.F.; Li, W.C. Rainfall-induced landslides in Hulu Kelang area, Malaysia. *Nat. Hazards* **2014**, *70*, 353–375. [[CrossRef](#)]
14. Huang, F.; Chen, J.; Liu, W.; Huang, J.; Hong, H.; Chen, W. Regional rainfall-induced landslide hazard warning based on landslide susceptibility mapping and a critical rainfall threshold. *Geomorphology* **2022**, *408*, 108236. [[CrossRef](#)]
15. Song, K.; Wang, F.; Yi, Q.; Lu, S. Landslide deformation behavior influenced by water level fluctuations of the Three Gorges Reservoir (China). *Eng. Geol.* **2018**, *247*, 58–68. [[CrossRef](#)]
16. Zhao, S.; Zeng, R.; Zhang, H.; Meng, X.; Zhang, Z.; Meng, X.; Wang, H.; Zhang, Y.; Liu, J. Impact of water level fluctuations on landslide deformation at Longyangxia reservoir, Qinghai province, China. *Remote Sens.* **2022**, *14*, 212. [[CrossRef](#)]
17. Zhang, Y.; Zhu, S.; Tan, J.; Li, L.; Yin, X. The influence of water level fluctuation on the stability of landslide in the Three Gorges Reservoir. *Arab. J. Geosci.* **2020**, *13*, 845. [[CrossRef](#)]
18. He, C.c.; Hu, X.l.; Xu, C.; Wu, S.s.; Zhang, H.; Liu, C. Model test of the influence of cyclic water level fluctuations on a landslide. *J. Mt. Sci.* **2020**, *17*, 191–202. [[CrossRef](#)]
19. Larsen, I.J.; Montgomery, D.R. Landslide erosion coupled to tectonics and river incision. *Nat. Geosci.* **2012**, *5*, 468–473. [[CrossRef](#)]
20. Cebulski, J. Impact of river erosion on variances in colluvial movement and type for landslides in the Polish Outer Carpathians. *Catena* **2022**, *217*, 106415. [[CrossRef](#)]
21. Premchitt, J.; Brand, E.; Phillipson, H. Landslides caused by rapid groundwater changes. *Geol. Soc. London Eng. Geol. Spec. Publ.* **1986**, *3*, 87–94. [[CrossRef](#)]
22. Corominas, J.; Moya, J.; Ledesma, A.; Lloret, A.; Gili, J.A. Prediction of ground displacements and velocities from groundwater level changes at the Vallcebre landslide (Eastern Pyrenees, Spain). *Landslides* **2005**, *2*, 83–96. [[CrossRef](#)]
23. Yin, Y.; Wang, F.; Sun, P. Landslide hazards triggered by the 2008 Wenchuan earthquake, Sichuan, China. *Landslides* **2009**, *6*, 139–152. [[CrossRef](#)]
24. Keefer, D.K. Investigating landslides caused by earthquakes—A historical review. *Surv. Geophys.* **2002**, *23*, 473–510. [[CrossRef](#)]
25. Shao, X.; Xu, C. Earthquake-induced landslides susceptibility assessment: A review of the state-of-the-art. *Nat. Hazards Res.* **2022**, *2*, 172–182. [[CrossRef](#)]
26. Huang, R.; Fan, X. The landslide story. *Nat. Geosci.* **2013**, *6*, 325–326. [[CrossRef](#)]
27. Korup, O.; Seidemann, J.; Mohr, C.H. Increased landslide activity on forested hillslopes following two recent volcanic eruptions in Chile. *Nat. Geosci.* **2019**, *12*, 284–289. [[CrossRef](#)]
28. Froude, M.J.; Petley, D.N. Global fatal landslide occurrence from 2004 to 2016. *Nat. Hazards Earth Syst. Sci.* **2018**, *18*, 2161–2181. [[CrossRef](#)]
29. Hussain, Y.; Schlögel, R.; Innocenti, A.; Hamza, O.; Iannucci, R.; Martino, S.; Havenith, H.B. Review on the Geophysical and UAV-Based Methods Applied to Landslides. *Remote Sens.* **2022**, *14*, 4564. [[CrossRef](#)]
30. Kang, Y.; Zhao, C.; Zhang, Q.; Lu, Z.; Li, B. Application of InSAR techniques to an analysis of the Guanling landslide. *Remote Sens.* **2017**, *9*, 1046. [[CrossRef](#)]
31. Sun, Q.; Zhang, L.; Ding, X.; Hu, J.; Li, Z.; Zhu, J. Slope deformation prior to Zhouqu, China landslide from InSAR time series analysis. *Remote Sens. Environ.* **2015**, *156*, 45–57. [[CrossRef](#)]
32. Van Natijne, A.; Bogaard, T.; van Leijen, F.; Hanssen, R.; Lindenbergh, R. World-wide InSAR sensitivity index for landslide deformation tracking. *Int. J. Appl. Earth Obs. Geoinf.* **2022**, *111*, 102829. [[CrossRef](#)]
33. Rosi, A.; Tofani, V.; Tanteri, L.; Tacconi Stefanelli, C.; Agostini, A.; Catani, F.; Casagli, N. The new landslide inventory of Tuscany (Italy) updated with PS-InSAR: Geomorphological features and landslide distribution. *Landslides* **2018**, *15*, 5–19. [[CrossRef](#)]
34. Xu, Q.; Zhao, B.; Dai, K.; Dong, X.; Li, W.; Zhu, X.; Yang, Y.; Xiao, X.; Wang, X.; Huang, J.; et al. Remote sensing for landslide investigations: A progress report from China. *Eng. Geol.* **2023**, *321*, 107156. [[CrossRef](#)]
35. Niethammer, U.; James, M.; Rothmund, S.; Travelletti, J.; Joswig, M. UAV-based remote sensing of the Super-Sauze landslide: Evaluation and results. *Eng. Geol.* **2012**, *128*, 2–11. [[CrossRef](#)]
36. Comert, R.; Avdan, U.; Gorum, T.; Nefeslioglu, H.A. Mapping of shallow landslides with object-based image analysis from unmanned aerial vehicle data. *Eng. Geol.* **2019**, *260*, 105264. [[CrossRef](#)]
37. Nex, F.; Remondino, F. UAV for 3D mapping applications: A review. *Appl. Geomat.* **2014**, *6*, 1–15. [[CrossRef](#)]
38. Johnson, S.E.; Haneberg, W.C.; Bryson, L.S.; Crawford, M.M. Measuring ground surface elevation changes in a slow-moving colluvial landslide using combinations of regional airborne lidar, UAV lidar and UAV photogrammetric surveys. *Q. J. Eng. Geol. Hydrogeol.* **2023**, *56*, qjegh2022–078. [[CrossRef](#)]
39. Li, W.; Zhao, B.; Xu, Q.; Yang, F.; Fu, H.; Dai, C.; Wu, X. Deformation characteristics and failure mechanism of a reactivated landslide in Leidashi, Sichuan, China, on 6 August 2019: An emergency investigation report. *Landslides* **2020**, *17*, 1405–1413. [[CrossRef](#)]
40. Zhou, C.; Ai, D.; Huang, W.; Xu, H.; Ma, L.; Chen, L.; Wang, L. Emergency Survey and Stability Analysis of a Rainfall-Induced Soil-Rock Mixture Landslide at Chongqing City, China. *Front. Earth Sci.* **2021**, *9*, 774200. [[CrossRef](#)]
41. Zheng, X.; Yang, X.; Ma, H.; Ren, G.; Yu, Z.; Yang, F.; Zhang, H.; Gao, W. Integrative Landslide Emergency Monitoring Scheme Based on GB-INSAR Interferometry, Terrestrial Laser Scanning and UAV Photography. *J. Phys. Conf. Ser.* **2019**, *1213*, 052069. [[CrossRef](#)]

42. Corominas, J.; van Westen, C.; Frattini, P.; Cascini, L.; Malet, J.P.; Fotopoulou, S.; Catani, F.; Van Den Eeckhaut, M.; Mavrouli, O.; Agliardi, F.; et al. Recommendations for the quantitative analysis of landslide risk. *Bull. Eng. Geol. Environ.* **2014**, *73*, 209–263. [[CrossRef](#)]
43. Qi, J.; Chen, H.; Chen, F. Extraction of landslide features in UAV remote sensing images based on machine vision and image enhancement technology. *Neural Comput. Appl.* **2022**, *34*, 12283–12297. [[CrossRef](#)]
44. Lucieer, A.; Jong, S.M.D.; Turner, D. Mapping landslide displacements using Structure from Motion (SfM) and image correlation of multi-temporal UAV photography. *Prog. Phys. Geogr. Earth Environ.* **2014**, *38*, 97–116. [[CrossRef](#)]
45. Saito, H.; Uchiyama, S.; Hayakawa, Y.S.; Obanawa, H. Landslides triggered by an earthquake and heavy rainfalls at Aso volcano, Japan, detected by UAS and SfM-MVS photogrammetry. *Prog. Earth Planet. Sci.* **2018**, *5*, 15. [[CrossRef](#)]
46. Saeed, A.; Younes, A.; Cai, C.; Cai, G. A Survey of Hybrid Unmanned Aerial Vehicles. *Prog. Aerosp. Sci.* **2018**, *98*, 91–105. [[CrossRef](#)]
47. Gantimurova, S.; Parshin, A.; Erofeev, V. GIS-based landslide susceptibility mapping of the Circum-Baikal railway in Russia using UAV data. *Remote Sens.* **2021**, *13*, 3629. [[CrossRef](#)]
48. Zhang, H.; Zhang, D.X. A combined survey to evaluate the thermal behavior of loess for a landslide-prone slope on the Heifangtai terrace in Northwest China. *J. Mt. Sci.* **2021**, *18*, 620. [[CrossRef](#)]
49. Melis, M.T.; Da Pelo, S.; Erbi, I.; Loche, M.; Deiana, G.; Demurtas, V.; Meloni, M.A.; Dessì, F.; Funedda, A.; Scaioni, M.; et al. Thermal remote sensing from UAVs: A review on methods in coastal cliffs prone to landslides. *Remote Sens.* **2020**, *12*, 1971. [[CrossRef](#)]
50. Delbridge, B.G.; Bürgmann, R.; Fielding, E.; Hensley, S.; Schulz, W.H. Three-dimensional surface deformation derived from airborne interferometric UAVSAR: Application to the Slumgullion Landslide. *J. Geophys. Res. Solid Earth* **2016**, *121*, 3951–3977. [[CrossRef](#)]
51. Bekar, A.; Antoniou, M.; Baker, C.J. Low-Cost, High-Resolution, Drone-Borne SAR Imaging. *IEEE Trans. Geosci. Remote Sens.* **2021**, *60*, 5208811. [[CrossRef](#)]
52. Moreira, L.; Lubeck, D.; Wimmer, C.; Castro, F.; Goes, J.A.; Castro, V.; Alcantara, M.; Ore, G.; Oliveira, L.P.; Bins, L.; et al. Drone-Borne P-band Single-Pass InSAR. In Proceedings of the 2020 IEEE Radar Conference (RadarConf20), Florence, Italy, 21–25 September 2020; pp. 1–6. [[CrossRef](#)]
53. Liu, C.; Liu, X.; Peng, X.; Wang, E.; Wang, S. Application of 3D-DDA integrated with unmanned aerial vehicle–laser scanner (UAV-LS) photogrammetry for stability analysis of a blocky rock mass slope. *Landslides* **2019**, *16*, 1645–1661. [[CrossRef](#)]
54. Cheng, Z.; Gong, W.; Tang, H.; Juang, C.H.; Deng, Q.; Chen, J.; Ye, X. UAV photogrammetry-based remote sensing and preliminary assessment of the behavior of a landslide in Guizhou, China. *Eng. Geol.* **2021**, *289*, 106172. [[CrossRef](#)]
55. Colica, E.; D’Amico, S.; Iannucci, R.; Martino, S.; Gauci, A.; Galone, L.; Galea, P.; Paciello, A. Using unmanned aerial vehicle photogrammetry for digital geological surveys: Case study of Selmun promontory, northern of Malta. *Environ. Earth Sci.* **2021**, *80*, 551. [[CrossRef](#)]
56. Chang, K.J.; Tseng, C.W.; Tseng, C.M.; Liao, T.C.; Yang, C.J. Application of Unmanned Aerial Vehicle (UAV)-Acquired Topography for Quantifying Typhoon-Driven Landslide Volume and Its Potential Topographic Impact on Rivers in Mountainous Catchments. *Appl. Sci.* **2020**, *10*, 6102. [[CrossRef](#)]
57. Frodella, W.; Gigli, G.; Morelli, S.; Lombardi, L.; Casagli, N. Landslide mapping and characterization through infrared thermography (IRT): Suggestions for a methodological approach from some case studies. *Remote Sens.* **2017**, *9*, 1281. [[CrossRef](#)]
58. Liu, D.; Hu, X.; Zhou, C.; Li, L.; He, C.; Sun, T. Model test study of a landslide stabilized with piles and evolutionary stage identification based on thermal infrared temperature analysis. *Landslides* **2020**, *17*, 1393–1404. [[CrossRef](#)]
59. Godone, D.; Allasia, P.; Borrelli, L.; Gullà, G. UAV and Structure from Motion Approach to Monitor the Maierato Landslide Evolution. *Remote Sens.* **2020**, *12*, 1039. [[CrossRef](#)]
60. Colomina, I.; Molina, P. Unmanned aerial systems for photogrammetry and remote sensing: A review. *ISPRS J. Photogramm. Remote Sens.* **2014**, *92*, 79–97. [[CrossRef](#)]
61. Robles-Kelly, A.; Huynh, C.P. *Imaging Spectroscopy for Scene Analysis*; Springer Science & Business Media: Berlin/Heidelberg, Germany, 2012.
62. Adam, E.; Mutanga, O.; Rugege, D. Multispectral and hyperspectral remote sensing for identification and mapping of wetland vegetation: A review. *Wetl. Ecol. Manag.* **2010**, *18*, 281–296. [[CrossRef](#)]
63. DJIEnterprise. DJI P4 Multispectral Specs. 2023. Available online: <https://www.dji.com/p4-multispectral/specs> (accessed on 15 January 2024).
64. Jaboyedoff, M.; Derron, M.H. Landslide analysis using laser scanners. In *Developments in Earth Surface Processes*; Elsevier: Amsterdam, The Netherlands, 2020; Volume 23, pp. 207–230. [[CrossRef](#)]
65. Vargas Rivero, J.R.; Gerbich, T.; Buschardt, B.; Chen, J. Data augmentation of automotive lidar point clouds under adverse weather situations. *Sensors* **2021**, *21*, 4503. [[CrossRef](#)]
66. Chen, S.; Wang, H.; Xu, F.; Jin, Y.Q. Target classification using the deep convolutional networks for SAR images. *IEEE Trans. Geosci. Remote Sens.* **2016**, *54*, 4806–4817. [[CrossRef](#)]
67. Vassilakis, E.; Fomelis, M.; Erkeki, A.; Kotsi, E.; Lekkas, E. Post-event surface deformation of Amyntaio slide (Greece) by complementary analysis of Remotely Piloted Airborne System imagery and SAR interferometry. *Appl. Geomat.* **2021**, *13*, 65–75. [[CrossRef](#)]

68. Zimmermann, F.; Eling, C.; Klingbeil, L.; Kuhlmann, H. Precise positioning of uavs—dealing with challenging rtk-gps measurement conditions during automated uav flights. *ISPRS Ann. Photogramm. Remote. Sens. Spat. Inf. Sci.* **2017**, *4*, 95–102. [[CrossRef](#)]
69. Zhou, H.; Xiong, H.L.; Liu, Y.; Tan, N.D.; Chen, L. Trajectory planning algorithm of UAV based on system positioning accuracy constraints. *Electronics* **2020**, *9*, 250. [[CrossRef](#)]
70. Queralta, J.P.; Almansa, C.M.; Schiano, F.; Floreano, D.; Westerlund, T. Uwb-based system for uav localization in gnss-denied environments: Characterization and dataset. In Proceedings of the 2020 IEEE/RSJ International Conference on Intelligent Robots and Systems (IROS), Las Vegas, NV, USA, 25–29 October 2020; pp. 4521–4528. [[CrossRef](#)]
71. Zhang, W.; Zhang, W. An efficient UAV localization technique based on particle swarm optimization. *IEEE Trans. Veh. Technol.* **2022**, *71*, 9544–9557. [[CrossRef](#)]
72. Couturier, A.; Akhloufi, M.A. A review on absolute visual localization for UAV. *Robot. Auton. Syst.* **2021**, *135*, 103666. [[CrossRef](#)]
73. Ferretti, A.; Prati, C.; Rocca, F. Permanent scatterers in SAR interferometry. *IEEE Trans. Geosci. Remote Sens.* **2001**, *39*, 8–20. [[CrossRef](#)]
74. Frey, O.; Werner, C.L.; Manconi, A.; Coscione, R. Measurement of surface displacements with a UAV-borne/car-borne L-band DInSAR system: System performance and use cases. In Proceedings of the 2021 IEEE International Geoscience and Remote Sensing Symposium IGARSS, Brussels, Belgium, 11–16 July 2021; pp. 628–631. [[CrossRef](#)]
75. Catani, F. Landslide detection by deep learning of non-nadir and crowdsourced optical images. *Landslides* **2021**, *18*, 1025–1044. [[CrossRef](#)]
76. Lian, X.G.; Li, Z.J.; Yuan, H.Y.; Liu, J.B.; Zhang, Y.J.; Liu, X.Y.; Wu, Y.R. Rapid identification of landslide, collapse and crack based on low-altitude remote sensing image of UAV. *J. Mt. Sci.* **2020**, *17*, 2915–2928. [[CrossRef](#)]
77. Han, L.; Duan, P.; Liu, J.; Li, J. Research on Landslide Trace Recognition by Fusing UAV-Based LiDAR DEM Multi-Feature Information. *Remote Sens.* **2023**, *15*, 4755. [[CrossRef](#)]
78. Liao, J.; Zhou, J.; Yang, W. Comparing LiDAR and SfM digital surface models for three land cover types. *Open Geosci.* **2021**, *13*, 497–504. [[CrossRef](#)]
79. Choi, S.K.; Ramirez, R.A.; Kwon, T.H. Acquisition of high-resolution topographic information in forest environments using integrated UAV-LiDAR system: System development and field demonstration. *Heliyon* **2023**, *9*, e20225. [[CrossRef](#)] [[PubMed](#)]
80. Westoby, M.J.; Brasington, J.; Glasser, N.F.; Hambrey, M.J.; Reynolds, J.M. ‘Structure-from-Motion’ photogrammetry: A low-cost, effective tool for geoscience applications. *Geomorphology* **2012**, *179*, 300–314. [[CrossRef](#)]
81. Leberl, F.; Irschara, A.; Pock, T.; Meixner, P.; Gruber, M.; Scholz, S.; Wiechert, A. Point clouds. *Photogramm. Eng. Remote Sens.* **2010**, *76*, 1123–1134. [[CrossRef](#)]
82. Fonstad, M.A.; Dietrich, J.T.; Courville, B.C.; Jensen, J.L.; Carbonneau, P.E. Topographic structure from motion: A new development in photogrammetric measurement. *Earth Surf. Process. Landforms* **2013**, *38*, 421–430. [[CrossRef](#)]
83. Sanz-Ablanedo, E.; Chandler, J.H.; Rodríguez-Pérez, J.R.; Ordóñez, C. Accuracy of unmanned aerial vehicle (UAV) and SfM photogrammetry survey as a function of the number and location of ground control points used. *Remote Sens.* **2018**, *10*, 1606. [[CrossRef](#)]
84. Yordanov, V.; Biagi, L.; Truong, X.; Brovelli, M. Landslide surveys using low-cost UAV and FOSS photogrammetric workflow. *Int. Arch. Photogramm. Remote Sens. Spat. Inf. Sci.* **2022**, *43*, 493–499. [[CrossRef](#)]
85. Martínez-Carricondo, P.; Agüera-Vega, F.; Carvajal-Ramírez, F.; Mesas-Carrascosa, F.J.; García-Ferrer, A.; Pérez-Porras, F.J. Assessment of UAV-photogrammetric mapping accuracy based on variation of ground control points. *Int. J. Appl. Earth Obs. Geoinf.* **2018**, *72*, 1–10. [[CrossRef](#)]
86. Ludwig, M.; M. Runge, C.; Friess, N.; Koch, T.L.; Richter, S.; Seyfried, S.; Wraase, L.; Lobo, A.; Sebastià, M.T.; Reudenbach, C.; et al. Quality assessment of photogrammetric methods—A workflow for reproducible UAS orthomosaics. *Remote Sens.* **2020**, *12*, 3831. [[CrossRef](#)]
87. Szypuła, B. Accuracy of UAV-based DEMs without ground control points. *Geoinformatica* **2023**, *28*, 1–28. [[CrossRef](#)]
88. Ouédraogo, M.M.; Degré, A.; Debouche, C.; Lisein, J. The evaluation of unmanned aerial system-based photogrammetry and terrestrial laser scanning to generate DEMs of agricultural watersheds. *Geomorphology* **2014**, *214*, 339–355. [[CrossRef](#)]
89. Sona, G.; Pinto, L.; Pagliari, D.; Passoni, D.; Gini, R. Experimental analysis of different software packages for orientation and digital surface modelling from UAV images. *Earth Sci. Inform.* **2014**, *7*, 97–107. [[CrossRef](#)]
90. James, M.R.; Robson, S. Straightforward reconstruction of 3D surfaces and topography with a camera: Accuracy and geoscience application. *J. Geophys. Res. Earth Surf.* **2012**, *117*. [[CrossRef](#)]
91. Carrivick, J.L.; Smith, M.W.; Quincey, D.J. *Structure from Motion in the Geosciences*; John Wiley & Sons: Hoboken, NJ, USA, 2016.
92. Peppas, M.V.; Mills, J.P.; Moore, P.; Miller, P.E.; Chambers, J.E. Accuracy Assessment of a UAV-BASED Landslide Monitoring System. *ISPRS Int. Arch. Photogramm. Remote Sens. Spat. Inf. Sci.* **2016**, *XLI-B5*, 895–902. [[CrossRef](#)]
93. Fernández, T.; Pérez, J.; Cardenal, J.; Gómez, J.; Colomo, C.; Delgado, J. Analysis of Landslide Evolution Affecting Olive Groves Using UAV and Photogrammetric Techniques. *Remote Sens.* **2016**, *8*, 837. [[CrossRef](#)]
94. Ma, S.; Xu, C.; Shao, X.; Zhang, P.; Liang, X.; Tian, Y. Geometric and kinematic features of a landslide in Mabian Sichuan, China, derived from UAV photography. *Landslides* **2019**, *16*, 373–381. [[CrossRef](#)]
95. Bentley, M.J.; Foster, J.M.; Potvin, J.J.; Bevan, G.; Sharp, J.; Woeller, D.J.; Take, W.A. Surface displacement expression of progressive failure in a sensitive clay landslide observed with long-term UAV monitoring. *Landslides* **2023**, *20*, 531–546. [[CrossRef](#)]

96. Wheaton, J.M. Uncertainty in Morphological Sediment Budgeting of Rivers. Ph.D. Thesis, University of Southampton, Southampton, UK, 2008.
97. Girardeau-Montaut, D.; Roux, M.; Marc, R.; Thibault, G. Change detection on points cloud data acquired with a ground laser scanner. *Int. Arch. Photogramm. Remote Sens. Spat. Inf. Sci.* **2005**, *36*, W19.
98. Cignoni, P.; Rocchini, C.; Scopigno, R. Metro: Measuring error on simplified surfaces. In *Computer Graphics Forum*; Wiley Online Library: Oxford, UK, 1998; Volume 17, pp. 167–174. [[CrossRef](#)]
99. Lague, D.; Brodu, N.; Leroux, J. Accurate 3D comparison of complex topography with terrestrial laser scanner: Application to the Rangitikei canyon (NZ). *ISPRS J. Photogramm. Remote Sens.* **2013**, *82*, 10–26. [[CrossRef](#)]
100. Gojcic, Z.; Zhou, C.; Wieser, A. F2S3: Robustified determination of 3D displacement vector fields using deep learning. *J. Appl. Geod.* **2020**, *14*, 177–189. [[CrossRef](#)]
101. Gojcic, Z.; Schmid, L.; Wieser, A. Dense 3D displacement vector fields for point cloud-based landslide monitoring. *Landslides* **2021**, *18*, 3821–3832. [[CrossRef](#)]
102. Andresen, C.G.; Schultz-Fellenz, E.S. Change Detection Applications in the Earth Sciences Using UAS-Based Sensing: A Review and Future Opportunities. *Drones* **2023**, *7*, 258. [[CrossRef](#)]
103. Al-Rawabdeh, A.; He, F.; Moussa, A.; El-Sheimy, N.; Habib, A. Using an unmanned aerial vehicle-based digital imaging system to derive a 3D point cloud for landslide scarp recognition. *Remote Sens.* **2016**, *8*, 95. [[CrossRef](#)]
104. Peng, D.; Xu, Q.; Liu, F.; He, Y.; Zhang, S.; Qi, X.; Zhao, K.; Zhang, X. Distribution and failure modes of the landslides in Heitai terrace, China. *Eng. Geol.* **2018**, *236*, 97–110. [[CrossRef](#)]
105. Qiu, H.; Cui, P.; Regmi, A.D.; Hu, S.; Wang, X.; Zhang, Y. The effects of slope length and slope gradient on the size distributions of loess slides: Field observations and simulations. *Geomorphology* **2018**, *300*, 69–76. [[CrossRef](#)]
106. Hu, S.; Qiu, H.; Pei, Y.; Cui, Y.; Xie, W.; Wang, X.; Yang, D.; Tu, X.; Zou, Q.; Cao, P.; et al. Digital terrain analysis of a landslide on the loess tableland using high-resolution topography data. *Landslides* **2019**, *16*, 617–632. [[CrossRef](#)]
107. Lo, C.M.; Li, H.H.; Ke, C.C. Kinematic model of a translational slide in the Cidu section of the Formosan Freeway. *Landslides* **2016**, *13*, 141–151. [[CrossRef](#)]
108. Gao, Y.; Yin, Y.; Li, B.; Feng, Z.; Wang, W.; Zhang, N.; Xing, A. Characteristics and numerical runout modeling of the heavy rainfall-induced catastrophic landslide–debris flow at Sanxicun, Dujiangyan, China, following the Wenchuan Ms 8.0 earthquake. *Landslides* **2017**, *14*, 1361–1374. [[CrossRef](#)]
109. Scaringi, G.; Fan, X.; Xu, Q.; Liu, C.; Ouyang, C.; Domènech, G.; Yang, F.; Dai, L. Some considerations on the use of numerical methods to simulate past landslides and possible new failures: The case of the recent Xinmo landslide (Sichuan, China). *Landslides* **2018**, *15*, 1359–1375. [[CrossRef](#)]
110. Ouyang, C.; An, H.; Zhou, S.; Wang, Z.; Su, P.; Wang, D.; Cheng, D.; She, J. Insights from the failure and dynamic characteristics of two sequential landslides at Baige village along the Jinsha River, China. *Landslides* **2019**, *16*, 1397–1414. [[CrossRef](#)]
111. Lin, M.L.; Chen, Y.C.; Tseng, Y.H.; Chang, K.J.; Wang, K.L. Investigation of Geological Structures Using UAV Lidar and Its Effects on the Failure Mechanism of Deep-Seated Landslide in Lantai Area, Taiwan. *Appl. Sci.* **2021**, *11*, 10052. [[CrossRef](#)]
112. Ali, S.; Biermanns, P.; Haider, R.; Reicherter, K. Landslide susceptibility mapping by using GIS along the China–Pakistan economic corridor (Karakoram Highway), Pakistan. *Nat. Hazards Earth Syst. Sci.* **2018**, *11*, 131–148.
113. Meten, M.; PrakashBhandary, N.; Yatabe, R. Effect of landslide factor combinations on the prediction accuracy of landslide susceptibility maps in the Blue Nile Gorge of Central Ethiopia. *Geoenviron. Disasters* **2015**, *2*, 9. [[CrossRef](#)]
114. Vojteková, J.; Vojtek, M. Assessment of landslide susceptibility at a local spatial scale applying the multi-criteria analysis and GIS: a case study from Slovakia. *Geomat. Nat. Hazards Risk* **2020**, *11*, 131–148. [[CrossRef](#)]
115. Kakavas, M.P.; Nikolakopoulos, K.G. Digital elevation models of rockfalls and landslides: A review and meta-analysis. *Geosciences* **2021**, *11*, 256. [[CrossRef](#)]
116. Tempa, K.; Peljor, K.; Wangdi, S.; Ghalley, R.; Jamtsho, K.; Ghalley, S.; Pradhan, P. UAV technique to localize landslide susceptibility and mitigation proposal: A case of Rinchening Goenpa landslide in Bhutan. *Nat. Hazards Res.* **2021**, *1*, 171–186. [[CrossRef](#)]
117. Bhatt, B.P.; Awasthi, K.D.; Heyojoo, B.P.; Silwal, T.; Kafle, G. Using geographic information system and analytical hierarchy process in landslide hazard zonation. *Appl. Ecol. Environ. Sci.* **2013**, *1*, 14–22. [[CrossRef](#)]
118. Song, Y.; Gong, J.; Gao, S.; Wang, D.; Cui, T.; Li, Y.; Wei, B. Susceptibility assessment of earthquake-induced landslides using Bayesian network: A case study in Beichuan, China. *Comput. Geosci.* **2012**, *42*, 189–199. [[CrossRef](#)]
119. Chae, B.G.; Park, H.J.; Catani, F.; Simoni, A.; Berti, M. Landslide prediction, monitoring and early warning: A concise review of state-of-the-art. *Geosci. J.* **2017**, *21*, 1033–1070. [[CrossRef](#)]
120. Ma, S.; Wei, J.; Xu, C.; Shao, X.; Xu, S.; Chai, S.; Cui, Y. UAV survey and numerical modeling of loess landslides: An example from Zaoling, southern Shanxi Province, China. *Nat. Hazards* **2020**, *104*, 1125–1140. [[CrossRef](#)]
121. Huang, A.B.; Lee, J.T.; Ho, Y.T.; Chiu, Y.F.; Cheng, S.Y. Stability monitoring of rainfall-induced deep landslides through pore pressure profile measurements. *Soils Found.* **2012**, *52*, 737–747. [[CrossRef](#)]
122. Toll, D.; Lourenço, S.; Mendes, J.; Gallipoli, D.; Evans, F.; Augarde, C.; Cui, Y.J.; Tang, A.; Rojas, J.; Pagano, L.; et al. *Soil Suction Monitoring for Landslides and Slopes*; Geological Society of London: London, UK, 2011. [[CrossRef](#)]
123. Sestras, P.; Bilasco, S.; Rosca, S.; Dudic, B.; Hysa, A.; Spalevic, V. Geodetic and UAV monitoring in the sustainable management of shallow landslides and erosion of a susceptible urban environment. *Remote Sens.* **2021**, *13*, 385. [[CrossRef](#)]

124. Mazzanti, P.; Caporossi, P.; Brunetti, A.; Mohammadi, F.I.; Bozzano, F. Short-term geomorphological evolution of the Poggio Baldi landslide upper scarp via 3D change detection. *Landslides* **2021**, *18*, 2367–2381. [[CrossRef](#)]
125. Cai, J.; Wang, C.; Zhang, L. Analysis of Mass Wasting Processes in the Slumgullion Landslide Using Multi-Track Time-Series UAVSAR Images. *Remote Sens.* **2023**, *15*, 4746. [[CrossRef](#)]
126. Hu, X.; Bürgmann, R.; Fielding, E.J.; Lee, H. Internal kinematics of the Slumgullion landslide (USA) from high-resolution UAVSAR InSAR data. *Remote Sens. Environ.* **2020**, *251*, 112057. [[CrossRef](#)]
127. Molan, Y.E.; Lohman, R.B. A Pattern-Based Strategy for InSAR Phase Unwrapping and Application to Two Landslides in Colorado. *J. Geophys. Res. Solid Earth* **2023**, *128*, e2022JB025761. [[CrossRef](#)]
128. Chowdhury, R.; Zhang, S. Tension cracks and slope failure. In *Slope Stability Engineering Developments and Applications: Proceedings of the International Conference on Slope Stability Organized by the Institution of Civil Engineers and Held on the Isle of Wight on 15–18 April 1991*; Thomas Telford Publishing: London, UK, 1991; pp. 27–32. [[CrossRef](#)]
129. Khattak, G.A.; Owen, L.A.; Kamp, U.; Harp, E.L. Evolution of earthquake-triggered landslides in the Kashmir Himalaya, northern Pakistan. *Geomorphology* **2010**, *115*, 102–108. [[CrossRef](#)]
130. Stumpf, A.; Malet, J.P.; Kerle, N.; Niethammer, U.; Rothmund, S. Image-based mapping of surface fissures for the investigation of landslide dynamics. *Geomorphology* **2013**, *186*, 12–27. [[CrossRef](#)]
131. Xu, L.; Dai, F.; Tham, L.; Zhou, Y.; Wu, C. Investigating landslide-related cracks along the edge of two loess platforms in northwest China. *Earth Surf. Process. Landf.* **2012**, *37*, 1023–1033. [[CrossRef](#)]
132. Tang, H.; Wasowski, J.; Juang, C.H. Geohazards in the three Gorges Reservoir Area, China—Lessons learned from decades of research. *Eng. Geol.* **2019**, *261*, 105267. [[CrossRef](#)]
133. Wang, H.; Nie, D.; Tuo, X.; Zhong, Y. Research on crack monitoring at the trailing edge of landslides based on image processing. *Landslides* **2020**, *17*, 985–1007. [[CrossRef](#)]
134. Vivaldi, V.; Bordoni, M.; Mineo, S.; Crozi, M.; Pappalardo, G.; Meisina, C. Airborne combined photogrammetry—Infrared thermography applied to landslide remote monitoring. *Landslides* **2023**, *20*, 297–313. [[CrossRef](#)]
135. Baroň, I.; Bečkovský, D.; Míča, L. Application of infrared thermography for mapping open fractures in deep-seated rockslides and unstable cliffs. *Landslides* **2014**, *11*, 15–27. [[CrossRef](#)]
136. Iwaszenko, S.; Kalisz, P.; Słota, M.; Rudzki, A. Detection of natural gas leakages using a laser-based methane sensor and uav. *Remote Sens.* **2021**, *13*, 510. [[CrossRef](#)]
137. Gómez, C.; Green, D.R. Small unmanned airborne systems to support oil and gas pipeline monitoring and mapping. *Arab. J. Geosci.* **2017**, *10*, 202. [[CrossRef](#)]
138. Marinos, V.; Stoumpos, G.; Papazachos, C. Landslide hazard and risk assessment for a natural gas pipeline project: The case of the Trans Adriatic Pipeline, Albania Section. *Geosciences* **2019**, *9*, 61. [[CrossRef](#)]
139. Nyman, D.J.; Lee, E.M.; Audibert, J.M. Mitigating geohazards for international pipeline projects: Challenges and lessons learned. In *Proceedings of the 2008 7th International Pipeline Conference, Calgary, AB, Canada, 29 September–3 October 2008*; Volume 48593, pp. 639–648. [[CrossRef](#)]
140. DJIEnterprise. DJI Records More Than 1000 People Rescued by Drones Globally. 2023. Available online: <https://www.dji.com/newsroom/news/dji-records-more-than-1000-people-rescued-by-drones-globally> (accessed on 15 January 2024).
141. Zhou, J.w.; Jiang, N.; Li, H.b. Automatic discontinuity identification and quantitative monitoring of unstable blocks using terrestrial laser scanning in large landslide during emergency disposal. *Landslides* **2023**. [[CrossRef](#)]
142. He, K.; Liu, B.; Hu, X. Preliminary reports of a catastrophic landslide occurred on August 21, 2020, in Hanyuan County, Sichuan Province, China. *Landslides* **2021**, *18*, 503–507. [[CrossRef](#)]
143. Guo, F.Y.; Meng, X.M.; Qi, T.J.; Dijkstra, T.; Thorkildsen, J.K.; Yue, D.X.; Chen, G.; Zhang, Y.; Dou, X.D.; Shi, P.Q. Rapid onset hazards, fault-controlled landslides and multi-method emergency decision-making. *J. Mt. Sci.* **2022**, *19*, 1357–1369. [[CrossRef](#)]
144. Jiang, N.; Li, C.j.; Li, H.b.; Zhou, Z.d.; Lu, G.d.; Zhou, J.w. Preliminary analysis of a landslide-dammed lake induced by two consecutive earthquakes on June 1, 2022, Sichuan Province, China. *Landslides* **2022**, *19*, 2535–2538. [[CrossRef](#)]
145. Liu, B.; He, K.; Han, M.; Hu, X.; Ma, G.; Wu, M. Application of UAV and GB-SAR in Mechanism Research and Monitoring of Zhonghaicun Landslide in Southwest China. *Remote Sens.* **2021**, *13*, 1653. [[CrossRef](#)]
146. Zhao, B.; Zhang, H.; Hongjian, L.; Li, W.; Su, L.; He, W.; Zeng, L.; Qin, H.; Dhital, M.R. Emergency response to the reactivated Aniangzhai landslide resulting from a rainstorm-triggered debris flow, Sichuan Province, China. *Landslides* **2021**, *18*, 1115–1130. [[CrossRef](#)]
147. DUKOWITZ, Z. Landslide in Norway Leads to Largest European Drone Operation Ever, 200+ Hours of Flight Time Recorded. 2021. Available online: <https://uavcoach.com/ask-landslide-drone-operation/> (accessed on 15 January 2024).
148. Enterprise, D. Drones Were Critical for Search and Rescue during Norway’s Biggest Landslide Disaster. 2021. Available online: <https://enterprise-insights.dji.com/blog/let-drones-search-so-you-can-rescue-norway-landslide-m300> (accessed on 15 January 2024).
149. PIX4Dmapper. Drone Mapping Saves Lives in Landslides. 2017. Available online: <https://www.pix4d.com/blog/drone-mapping-saves-lives-rescuav-landslide-in-colombia/> (accessed on 15 January 2024).
150. Kangunde, V.; Jamisola, R.S.; Theophilus, E.K. A review on drones controlled in real-time. *Int. J. Dyn. Control* **2021**, *9*, 1832–1846. [[CrossRef](#)]

151. Jiang, N.; Li, H.B.; Li, C.J.; Xiao, H.X.; Zhou, J.W. A Fusion Method Using Terrestrial Laser Scanning and Unmanned Aerial Vehicle Photogrammetry for Landslide Deformation Monitoring Under Complex Terrain Conditions. *IEEE Trans. Geosci. Remote Sens.* **2022**, *60*, 4707214. [[CrossRef](#)]
152. Yun, L.; Zhang, X.; Zheng, Y.; Wang, D.; Hua, L. Enhance the Accuracy of Landslide Detection in UAV Images Using an Improved Mask R-CNN Model: A Case Study of Sanming, China. *Sensors* **2023**, *23*, 4287. [[CrossRef](#)] [[PubMed](#)]
153. Nota, E.; Nijland, W.; de Haas, T. Improving UAV-SfM time-series accuracy by co-alignment and contributions of ground control or RTK positioning. *Int. J. Appl. Earth Obs. Geoinf.* **2022**, *109*, 102772. [[CrossRef](#)]
154. Rodríguez-Caballero, E.; Rodríguez-Lozano, B.; Segura-Tejada, R.; Blanco-Sacristán, J.; Cantón, Y. Landslides on dry badlands: UAV images to identify the drivers controlling their unexpected occurrence on vegetated hillslopes. *J. Arid. Environ.* **2021**, *187*, 104434. [[CrossRef](#)]
155. Büschelberger, M.; Wilk, J.; Hergarten, S.; Preusser, F. Size–frequency distribution of shallow landslides in the Black Forest, Germany. *Earth Surf. Process. Landf.* **2022**, *47*, 179–192. [[CrossRef](#)]
156. Dille, A.; Kervyn, F.; Mugaruka Bibentyo, T.; Delvaux, D.; Ganza, G.B.; Ilombe Mawe, G.; Kalikone Buzera, C.; Safari Nakito, E.; Moeyersons, J.; Monsieurs, E.; et al. Causes and triggers of deep-seated hillslope instability in the tropics – Insights from a 60-year record of Ikoma landslide (DR Congo). *Geomorphology* **2019**, *345*, 106835. [[CrossRef](#)]
157. Koutalakis, P.D.; Tzoraki, O.A.; Prazioutis, G.I.; Gkiatas, G.T.; Zaimis, G.N. Can Drones Map Earth Cracks? Landslide Measurements in North Greece Using UAV Photogrammetry for Nature-Based Solutions. *Sustainability* **2021**, *13*, 4697. [[CrossRef](#)]
158. Șandric, I.; Irimia, R.; Ilinca, V.; Chițu, Z.; Gheuca, I. Using UAV Time Series to Estimate Landslides’ Kinematics Uncertainties, Case Study: Chirlești Earthflow, Romania. *Remote Sens.* **2023**, *15*, 2161. [[CrossRef](#)]
159. Xu, Q.; Li, W.L.; Ju, Y.z.; Dong, X.j.; Peng, D.L. Multitemporal UAV-based photogrammetry for landslide detection and monitoring in a large area: A case study in the Heifangtai terrace in the Loess Plateau of China. *J. Mt. Sci.* **2020**, *17*, 1826–1839. [[CrossRef](#)]
160. Conforti, M.; Mercuri, M.; Borrelli, L. Morphological Changes Detection of a Large Earthflow Using Archived Images, LiDAR-Derived DTM, and UAV-Based Remote Sensing. *Remote Sens.* **2020**, *13*, 120. [[CrossRef](#)]
161. Zárate, B.A.; El Hamdouni, R.; Fernández Del Castillo, T. Characterization and Analysis of Landslide Evolution in Intramountain Areas in Loja (Ecuador) Using RPAS Photogrammetric Products. *Remote Sens.* **2023**, *15*, 3860. [[CrossRef](#)]

Disclaimer/Publisher’s Note: The statements, opinions and data contained in all publications are solely those of the individual author(s) and contributor(s) and not of MDPI and/or the editor(s). MDPI and/or the editor(s) disclaim responsibility for any injury to people or property resulting from any ideas, methods, instructions or products referred to in the content.